

8-1-2016

Nanomaterials for Solar Distillation Technology

Jack Warren Stoddard Cheney
University of Nevada, Las Vegas

Follow this and additional works at: <https://digitalscholarship.unlv.edu/thesesdissertations>



Part of the [Mechanical Engineering Commons](#)

Repository Citation

Cheney, Jack Warren Stoddard, "Nanomaterials for Solar Distillation Technology" (2016). *UNLV Theses, Dissertations, Professional Papers, and Capstones*. 2775.
<http://dx.doi.org/10.34917/9302928>

This Thesis is protected by copyright and/or related rights. It has been brought to you by Digital Scholarship@UNLV with permission from the rights-holder(s). You are free to use this Thesis in any way that is permitted by the copyright and related rights legislation that applies to your use. For other uses you need to obtain permission from the rights-holder(s) directly, unless additional rights are indicated by a Creative Commons license in the record and/or on the work itself.

This Thesis has been accepted for inclusion in UNLV Theses, Dissertations, Professional Papers, and Capstones by an authorized administrator of Digital Scholarship@UNLV. For more information, please contact digitalscholarship@unlv.edu.

NANOMATERIALS FOR SOLAR DISTILLATION TECHNOLOGY

By

Jack W.S. Cheney

Bachelor of Science in Mechanical Engineering
University of Nevada, Las Vegas
2014

A thesis submitted in partial fulfillment
of the requirements for the

Master of Science in Engineering – Mechanical Engineering

Department of Mechanical Engineering
Howard R. Hughes College of Engineering
The Graduate College

University of Nevada, Las Vegas
May 2016



Thesis Approval

The Graduate College
The University of Nevada, Las Vegas

May 13, 2016

This thesis prepared by

Jack W.S. Cheney

entitled

Nanomaterials for Solar Distillation Technology

is approved in partial fulfillment of the requirements for the degree of

Master of Science in Engineering – Mechanical Engineering
Department of Mechanical Engineering

Jaeyun Moon, Ph.D.
Examination Committee Chair

Kathryn Hausbeck Korgan, Ph.D.
Graduate College Interim Dean

Robert Boehm, Ph.D.
Examination Committee Member

Yi-Tung Chen, Ph.D.
Examination Committee Member

Daniel Gerrity, Ph.D.
Graduate College Faculty Representative

Abstract

NANOMATERIALS FOR SOLAR DISTILLATION TECHNOLOGY

By
Jack Cheney

Dr. Jaeyun Moon, Examination Committee Chair
Professor of Mechanical Engineering
University of Nevada, Las Vegas

Water is the most important resource for mankind. Yet, 97% of the earth's surface water is seawater in the oceans and only 3% is fresh water in ground water. Therefore, different kinds of water desalination and treatment technologies have been developed, and water distillation is a basic process of evaporating water in order to leave behind impurities such as minerals, pollutants, and other contaminants. Although distillation is known as an effective water treatment process that removes many kinds of bacteria and inorganic chemicals and heavy metals, a large amount of conventional energy and non-renewable resources are consumed for this process. The objective of this thesis is to develop water distillation technology that uses plentiful and free solar energy by utilizing different functional nanomaterials. Double layered functional materials (exfoliated graphite and carbon foam) were used for sunlight absorption and heat localization which enable significantly improved water evaporation efficiency. A test chamber was built for heat loss minimization through the side surfaces and an indoor cost-effective solar simulator was designed to generate similar incident lights of solar irradiation using FRED simulation to verify the results. This indoor solar simulator allowed to perform consistent and reliable tests. The double layered materials were characterized using electron microscopes and various material analysis. The performance of the developed system was examined by measuring the temperature profile of the bulk water and the mass of evaporated water. The purified water produced by the developed distillation system was examined using two different analysis methods. The double layered

functional materials localize heat within top layer and it led to enhance the evaporation rate by a factor of five (5) under one (1) sun irradiation. The heat localization was also demonstrated using a heat transfer simulation. Although a further water quality study needs to be carried out, it was demonstrated that the developed system can be promising in a next generation solar distillation process.

Keywords: carbon, nanomaterials, solar distillation, solar simulation, steam generation, water collecting

Acknowledgements

I would like to thank Dr. Jaeyun Moon and my entire committee for their time and help in developing this thesis. I would also like to thank Dale Karas, Hyeunhwan An, and Soroosh Mortazavian for their support both in the lab and in understanding new parts of this project that a mechanical engineering education alone can't provide. I also would like to thank the NEXUS SEED Grant for the support provided by its funding. Lastly, I would like to thank my many friends and family for their support and help in this project as I would not have completed this project without them.

Table of Contents

Abstract	iii
Acknowledgements	v
List of Tables	viii
List of Figures	ix
Chapter 1: Introduction	1
1.1 Motivation	1
1.2 Background	2
1.2 Technical Approaches	7
1.3 Objectives	9
1.4 Organization	10
Chapter 2: Functional materials for Heat Localization	11
2.1 Exfoliated Graphite	11
2.1.1 Fabrication	12
2.1.2 Material Characterization	13
2.2 Treated Carbon Foam	15
2.2.1 Fabrication	16
2.2.2 Material Characterization	16
Chapter 3: Cost-Effective Solar Simulator	18
3.1 Design Specifications	19
3.2 FRED Simulation	20
3.3 Experimental and Spectrometer Recordings	24
Chapter 4: Water Evaporation Efficiency	33
4.1 Design Specifications	34
4.4 Experimental Procedure	34
4.2 LabVIEW Programming	37
4.3 Heat Transfer Modeling	37
4.5 Results and Discussion	39
Chapter 5: Water Purification	44
5.1 Aqualog Hardware and Software	45
5.2 Fluorescence and UV-VIS Spectroscopy	45
5.3 Results and Discussion	46

Chapter 6: Conclusions and Future Work.....	51
6.1 Conclusions	51
6.2 Future Work	51
Appendix.....	55
Appendix A: Material Candidates.....	55
Appendix B: LabVIEW Block Diagrams.....	56
Appendix C: Autodesk Inventor Drawings for Test Chamber.....	57
Appendix D: PLT Metal Halide Lamp Datasheet.....	58
Appendix E: Autodesk Inventor Drawings for Metal Halide Lamp Setup.....	59
Appendix F: Optical Setup.....	62
Bibliography	63
Curriculum Vitae	66

List of Tables

Table 1: Researched water collectors for optimal design. 6
Table 2: Material properties for experimental setup..... 38
Table 3: 1 sun mass change recordings..... 41
Table 4: Various research nanomaterials candidates for solar distillation application..... 55

List of Figures

Figure 1: A solar still schematic design (Kalita et al., 2016).....	3
Figure 2: Schematic of double layered materials for solar distillation	8
Figure 3: A basic design schematic for testing the DLS.....	9
Figure 4: Reflectance results used to evaluate solar absorption of exfoliated graphite (Ghasemi et al., 2014)	12
Figure 5: SEM of exfoliated graphite at x100 resolution	13
Figure 6: SEM of exfoliated graphite at x10,000 resolution	14
Figure 7: Contact angle for 8 second synthesis exfoliated graphite	15
Figure 8: Contact angle for 12 second synthesis exfoliated graphite	15
Figure 9: SEM of treated carbon foam at x50 resolution.....	17
Figure 10: As purchased carbon foam (right) vs. acid treated carbon foam (left).....	17
Figure 11: Modeled and recorded values for metal halide spectroscopy output compared to natural sunlight.....	19
Figure 12: The source lamp with 100,000 rays being emitted.....	21
Figure 13: 50,000 Ray trace of first model for metal halide lamp with Mylar tunnel.....	22
Figure 14: Irradiance spread at 26 inches from source	23
Figure 15: Irradiance spread at 30 inches from source	24
Figure 16: Ballast wiring diagram for metal halide lamp.....	25
Figure 17: The physical working wiring for the HID setup.....	25
Figure 18: The metal halide simulated solar basic setup	26
Figure 19: Aluminum hollow cylinder with Mylar coating around inner surface	27
Figure 20: Measurement of angular offset for reflector and Mylar tunnel	27
Figure 21: 12.94 degree adjustment of bulb with reflector.....	28
Figure 22: Ray trace of 50,000 rays of adjusted source.....	29
Figure 23: Irradiance of adjusted source at 26 inches.....	30
Figure 24: Maximum positioning for the irradiance model at 26 inches offset.....	30
Figure 25: Final irradiance distribution of experimental metal halide source	32
Figure 26: Final x and y coordinates from center of lamp for optimal metal halide exposure.....	32
Figure 27: The full experimental setup ready for testing.....	37
Figure 28: Autodesk Simulation Mechanical temperature distribution	39
Figure 29: Results for 1 sun testing	40
Figure 30: Result for 1 sun water alone temperature distribution	42
Figure 31: Result for 1 sun exfoliated graphite temperature distribution	43
Figure 32: Result for 1 sun carbon foam temperature distribution.....	43
Figure 33: Result for 1 sun DLS temperature distribution	44
Figure 34: Distilled water on water collector	47
Figure 35: Contaminated potassium permanganate water (left) and final distilled water (right).	47
Figure 36: Initial EEM of potassium permanganate water in fluorescence.....	48
Figure 37: Result for EEM of distilled water from setup in fluorescence	49
Figure 38: Result for UV-VIS Spectroscopy of Potassium Permanganate distillation	50
Figure 39: Initial MFF wastewater fluorescence absorbance	52

Figure 40: Final fluorescence of MFF after activated carbon exposure	53
Figure 41: An example of an acrylic larger scale solar distiller	54
Figure 42: VI for mass change	56
Figure 43: VI for temperature recording	56
Figure 44: The test chamber model used for analysis with water and DLS	57
Figure 45: Datasheet for metal halide lamp provided by PLT	58
Figure 46: CAD model of the metal halide (ANSI: M59) light bulb	59
Figure 47: The reflector combined with the metal halide bulb	59
Figure 48: CAD drawings with dimensions for lamp with reflector	60
Figure 49: CAD drawing of Mylar tunnel	61
Figure 50: Optical setup for the spectrometer readings	62

Chapter 1: Introduction

1.1 Motivation

Fresh water of sufficient quantity is critical for humanity and all life. However, about 97% of the world's water is seawater in oceans with the last 3% as fresh water and only 0.3% is available surface water (Cohen-Tanugi et Al, 2012). The limited fresh water causes many problems including 900 million people not receiving water via cleaning facilities (Macedonio et al., 2012) and 3.3 million people who die from water shortage or contamination each year with continuous health problems in many regions. A water distillation process is effective to produce high quality water, but the main drawback of the existing systems is the high capital costs and the large energy consumption; in particular the conventional energy sources including coals, oils and fossil fuel takes a heavy toll on the environment.

The sun is also an invaluable resources needed for sustainable life on earth. It has existed and supplemented a cycle of life and death for this little blue planet for all forms of life be it small bacteria, human beings, or a given flora. The amount of energy in one hour of sunlight is enough to sustain the energy needs of all people on earth for one year (Lewis, 2007). It's simply a matter of harnessing its great power.

Mankind has learned to value these resources as the sun provides heat and light for the day while water provides nourishment in the form of hydration and food. An ongoing investigation is finding a way to use solar energy to obtain clean water (Fath, 1998) (Sampathkumar, 2010). A goal by the World Health Organization for 2005-2015 was to “halve...the proportion of people without sustainable access to safe drinking water and basic sanitation” (WHO, 2005). As time goes on, more and more fresh water becomes harder to obtain naturally in the environment as climate change and civilization takes its toll on all ecosystems and so producing clean water from

polluted sources is key. The WHO also discusses the use of solar disinfection as a point-of-use cleaning option using plastic bottles. Ultraviolet germicidal irradiation is already a promising attempt to incorporate solar energy into cleaning water. This is where solar distillation becomes a possible solution. The act of distilling water is in of itself an effective method of reducing pollutants in water simply by boiling it and collecting the steam that is generated via evaporation and condensation (one of water's invaluable cycles) (Tiwari, 2003). Laboratories have used this method to obtain sterile water for various testing procedures and produce a safe source of drinking water thanks to killing off any pathogens from the boiling process and leaving heavy metals behind as the water turns into steam. The research into this optimal process will be conducted because it is the best way to incorporate renewable energies into obtaining clean drinking water.

1.2 Background

Solar distillation in its basic form involves the use of the sun's energy and a means of water collecting. The most basic form that has gained popularity is the solar still (Kalita et al., 2016). Figure 1 shows an example of the device that uses principles of the phase change cycle for water making use of evaporation and condensation. It uses a simple absorbing surface such as glass to transfer solar energy towards a pool of water that is to be distilled (Al-Hayeka, 2004). The glass is sloped such that when the water collects and condensates on the surface, gravity will drive it down towards a collecting trough at the bottom of the glass. The box itself can be designed with different materials but the glass sloped surface is most important not only for its transparency but also for its thermal stability over time during exposure to the sun. Water can be continuously fed into the box as the basin decreases in volume throughout the day. A drainage pipe is used near the bottom of the still to allow water to drain into a cooler container. Analysis of the thermodynamics and the condensation design has been investigated with prototypes generating up to 40 liters of

freshwater per square meter (Koning, 2005). The life cycle of a well-designed solar still can be as long as 20 years with several applications based on the need. The cost is based on financial cost and the cost of energy. For a distillation system powered by conventional energy sources, it takes about 12.8 kilowatt-hours of energy to distill one gallon of water. This value, when compared with the approximate value of 10 cents per kilowatt-hour, results in a cost of \$1.28 per gallon of water distilled. This may sound like a small number, but when compared to generating several gallons of distilled water, this cost can add up quickly. Besides the financial cost, the energy cost cannot be made up as a non-renewable resource is used to produce water that, if the sun was used instead, could be obtained for free. The investment needed for an inexpensive solar still pays itself off quickly thanks to readily available materials and ease of access to clean energy.

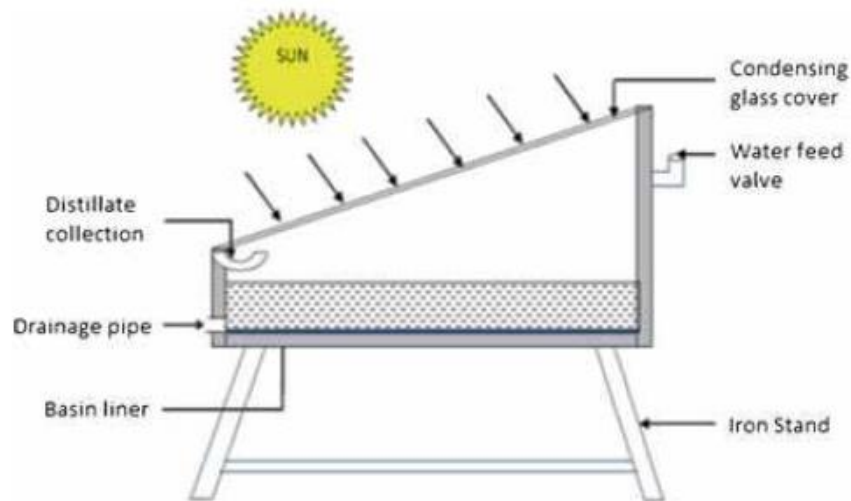


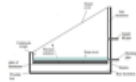
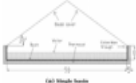
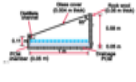
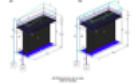
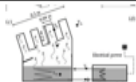
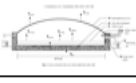

Figure 1: A solar still schematic design (Kalita et al., 2016)

The design has many different configurations to improve evaporation rate and condensate generation. This includes sponge cubes, still with integrated fins, flat plate collectors, mini solar ponds, wick type solar stills, and many others that go beyond the scope of this report. A summary of investigated configurations are provided in Table 1. The first design is based around the basic solar still discussed previously. This is essentially what modified solar stills are compared to for

performance as the efficiency of evaporation and water collecting are easily comparable for different designs (Kalita et al., 2016). The design varies across several sources reaching as low as 25% efficiency and as high as 60% efficiency in collecting water through the distillation process. The next design explores a double sloped single basin which essentially means it allows for more water to drain down another slope (Morad et al., 2015). Following after this is a design that incorporates phase change materials to store energy and prolong the distillation process (Ali, 2014). The efficiency is analyzed to be 57% when incorporating the PCM for thermal storage. Another configuration involved the use of vertical solar stills that allowed for condensate to cascade down either a single slope or double slope still in order to increase surface area (a consistent improvement goal for solar distillation design) (Sharon, 2015). A still that incorporates tower-like surfaces for increasing the area of condensation is also investigated (Bhardwaj et al., 2016). Up to 40% efficiency is obtained from the improved surface area. Another setup changed the shape of the glass into a round hemisphere design to see how the distillation process improved with and without flowing water spread over the cover glass (Arunkumar et al., 2012). The efficiency isn't too high though reaching 34% for the curved design. Finally, a pyramid configuration of the solar still was developed for a three dimensional approach to improve surface area of distillation (Taamneh, 2012). This produces a consistent 50% efficiency in collecting water from the extra surface area. Several of these designs are examined for three factors: efficiency, difficulty design, and cost shown in Table 1. Though the improvements suggested by the other research, the simple single slope seemed like a good control distiller for research purposes as the hope is to incorporate something new into a more basic design to see how it improves the overall distillation process. This is where nanomaterials became of interest for research purposes.

Nanomaterials, in particular nanoparticles, were already getting some early incorporation into solar distillation (Kabeel et al., 2014). One early example was using nanoparticles such as cuprous and aluminum oxide were tested with the goal of improving evaporation rate due to higher thermal conductivity. Cuprous oxide is recorded as having $76.5 \text{ W m}^{-1} \text{ K}^{-1}$ for a thermal conductivity while aluminum oxide has $46 \text{ W m}^{-1} \text{ K}^{-1}$ demonstrating how useful they can be for heating water with their high heat transfer coefficients. The improvement compared to water alone is usually around 30% which a promising value. Nanofluids have also been of interest as a floating absorber of solar energy (Elango et al., 2015). Zinc Oxide and Tin Oxide were investigated to see how well they improve distillation production with each one producing 12.67% and 18.63% more production than a normal still without water. They both have fairly close thermal conductivities of $0.6 \text{ W m}^{-2} \text{ K}^{-1}$. The reason given that this improves distillation is the temperature difference between the glass cover and the nanofluid absorbing more radiation. The reason these improve heat transfer and steam generation is the temperature difference that exists between the water surface and the bulk water volume. Despite these improvements, the efficiencies could be better given better materials and setup and so the optimal materials are investigated.

Table 1: Researched water collectors for optimal design.

Solar Water Distillation Designs Decision Matrix (Scale 1-5)							
Design	Title	Concept and Description	Difficulty	Cost	Efficiency (condensing vapor)	Total	Image
0	A review of solar energy driven desalination technologies	Normal Basic Solar Still, single slope with single collecting area	(1) Simple design for the basic needs of recovering water and requires very little in terms of design; very predictable results	(1) Notably the cheapest option since most other designs require more components added to this	(3) 25-60%	5	
1	Improving the double slope solar still performance by using flat-plate solar collector and cooling glass cover	Solar Still with a triangle style setup (two sloped surfaces)	(1) Requires attaching two pieces of glass or similar material together and adding another; still fairly easy design	(2) Requires twice the glass cover and a way to put them together	(2) 57%	4	
2	Modelling of solar distillation system with phase change material (PCM) storage medium	Solar Still, phase changing material, PCM underneath for continuous heating after sunset	(4) The challenge to find a way to use the phase changing material	(2) Similar to the basic design except using a PCM (cost may vary though)	(4) 39.6%	10	
3	Performance investigation and environmental analysis of active vertical solar distillation units	Double sided vertical solar still, water condenses down two walls	(2) Essentially an elevated basic solar still with the option of single or double slope for condensation collection	(3) Depends on the choice of single vs double slope, but the cost will be based on vertical size and the materials needed for the height	(2) Range of 35-55%	7	
4	Maximized production of water by increasing area of condensation surface for solar distillation	Takes basic solar still and adds "towers" to improve surface area and lose more heat	(3) might take time due to its complexity; creating these "towers" may prove challenging	(4) May be more costly due to the configuration and needing specific columns for this (may need to be custom made)	(2) 60%	9	
5	An experimental study on a hemispherical solar still	Two areas of collection, curved convex glass, basic solar still	(3) If the curved glass is easy enough to get, the difficulty of making this isn't much higher than a normal solar still	(3) Depends on the overall cost of the curved cover, but otherwise similar to normal solar still	(4) 34%	10	
6	Performance of pyramid-shaped solar still: Experimental study	Basic solar still with pyramid cover	(3) Similar to triangle setup, this requires figuring out how to attach these together and collect water on each side	(3) Cost of 4 glass covers, but still fairly cheap; may need to be custom made or cut (either by us or a provider)	(3) 50%	9	

1.2 Technical Approaches

Most recently, a group at MIT has been investigating the use of porous carbon materials in conjunction with this distillation process (Ghasemi et al., 2014). This article was chosen as a ground basis for this thesis investigation because the results are the most promising from a functional material approach. The sizable efficiency of 64% efficiency at just 1 sun for generating steam compared to other candidates generates a lot of promise in this particular material design. This article explores the use of sunlight as a means of heat localization by which the materials used are in a double layered structure (DLS) with one material on top of the other. Figure 2 shows the structure of the material to be used. The idea of absorbing and holding solar energy near the water surface is known as heat localization and is a study of interest for this project. A series of materials were investigated that are outlined in Appendix A. Their major properties including thermal conductivity, density, hydrophilicity (in order to allow water to pass through it easily), and solar absorption helped develop the design for a nanocomposite. Candidates were investigated as either filters for removing volatile organic compounds (VOCs) or heat insulators and absorbers of solar energy with their properties recovered from various online sources. As the goal is for these materials to possibly float on the surface of the water, a low density was very important and, if a material proved lacking in this property, it had to be discounted.

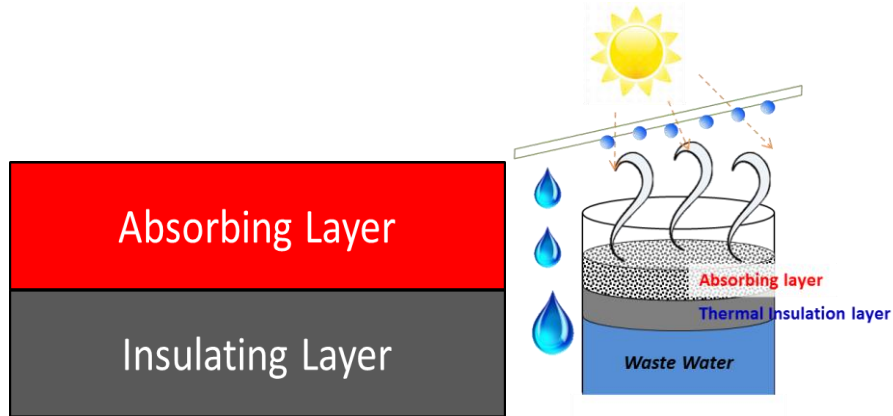


Figure 2: Schematic of double layered materials for solar distillation

A similar equipment setup to the article was used to evaluate evaporation efficiency of double layered materials. Details of experiments will be described in Chapter 4. The efficiency was determined by a simple formula:

$$\eta_{th} = \frac{\dot{m}h_{LV}}{C_{opt}q_i}$$

where \dot{m} denotes the mass flux [$\text{kg m}^{-2}\text{hr}^{-1}$], h_{LV} is total enthalpy of liquid-vapor phase change of water, C_{opt} is the optical concentration and q_i is the nominal solar irradiation 1 kWm^{-2} . Heat localization was to be investigated using a temperature gradient between the steaming surface and the underlying bulk water. Figure 3 shows how the plan is to measure mass change and temperature distribution over time in order to understand the efficiency of the material addition.

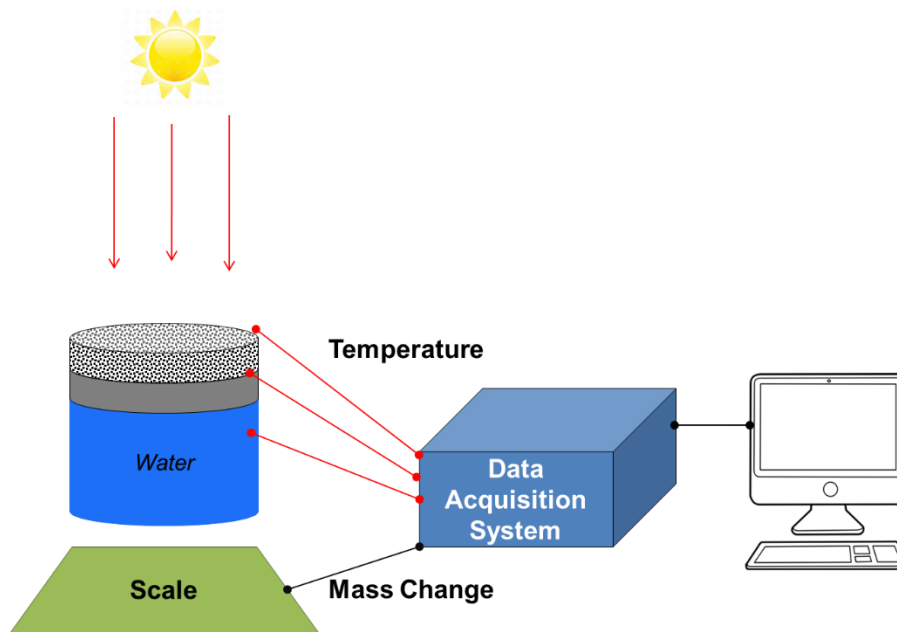


Figure 3: A basic design schematic for testing the DLS

The source of solar energy was simulated. A simulation of solar using metal halide lamps was also developed for an indoor laboratory setting in order to allow for reliable and consistent testing conditions. Due to the challenges of weather and time constraints, the cost-effective metal halide lamp became a primary source of providing power for the distillation process allowing for investigation as well into how reliable it is as a solar simulator.

A standard single basin solar still designed to scale is to be tested that allows the collecting of this water. In order to minimize the challenge of saturation, the goal is to design a small enough container that will facilitate the water being moved into a cooler chamber for collection.

1.3 Objectives

The objective of the solar distillation experiment is to determine the following:

- Utilize double layered functional materials for improving solar distillation
- Model solar energy using a simple, cost-effective simulator
- Determine the mass change and temperature distribution during testing

- Examine the efficiencies of the various testing setups
- Verify the purity of the water collected from this project

These general parameters shaped the scope of this project and helped define meaningful progress as research and testing was implemented.

1.4 Organization

In this thesis, sequential sections will outline the experimental process of this project. Chapter 2 will feature the properties and creation of the nanomaterials to be discussed and tested. Chapter 3 examines the FRED modeling of the project in order to see how the metal halide lamp works as a solar simulator for the experimental purposes. Chapter 4 explains the project setup with the goal of examining the experimental protocol and the results of testing in the form of mass change and temperature recording. Finally, the water testing is shown in chapter 5 with the Aqualog hardware being used for fluorescence excitation-emission testing as well as ultraviolet-visible absorbance to see the final quality of the distilled water.

Chapter 2: Functional materials for Heat Localization

The discussion of the double layered materials involved will be broken up into two categories. The first will be a discussion about the absorbing layer with exfoliated graphite. The second portion will detail the insulating layer that is the treated carbon foam. The materials will be evaluated for morphology based on for their ability to be hydrophilic for the purposes of this project.

2.1 Exfoliated Graphite

The requirements of the top absorbing layer of the DLS is 1) for high solar energy absorption across a broad wavelength spectrum of the sun and 2) hydrophilicity. In this research, exfoliated graphite was utilized at the top layer. This material incorporates properties that favor absorption of solar energy based on prior studies (Ghasemi et al., 2014). Figure 4 shows the absorption spectrum recorded for this particular form of graphite. The low reflectance of approximately 3% throughout indicates a high absorption of 97% within the desired solar spectrum. It also can be made hydrophilic in order for water to pass through it as steam is generated. Floating on the surface is also desirable but the insulating layer will help with this property which to be discussed later.

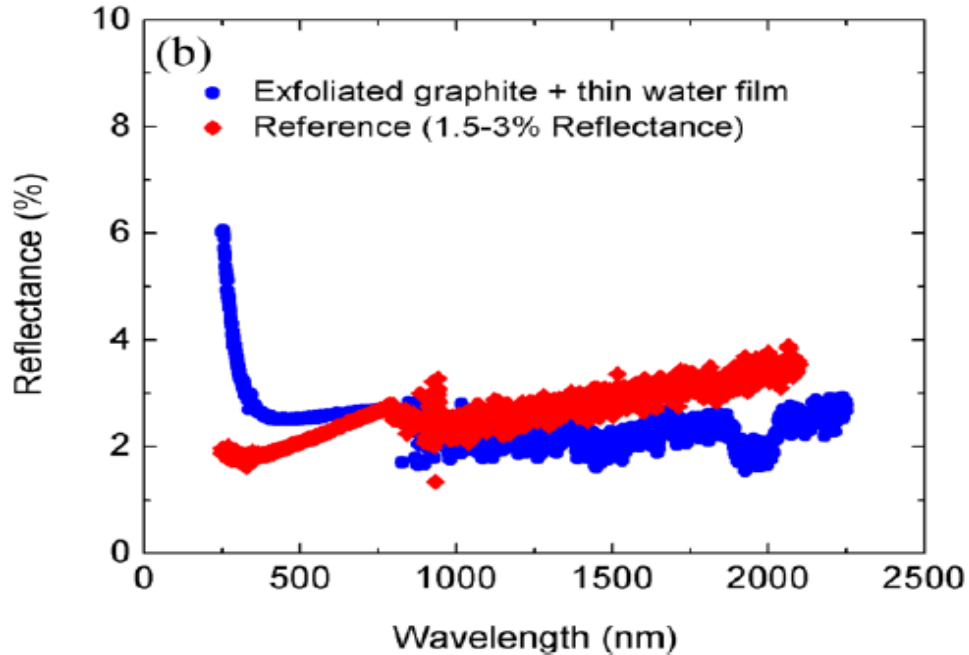


Figure 4: Reflectance results used to evaluate solar absorption of exfoliated graphite (Ghasemi et al., 2014)

2.1.1 Fabrication

Synthesis of the exfoliated graphite followed a simple process of first combining 1 gram of potassium permanganate (KMnO_4) with 0.5 grams of graphite flakes which were both purchased from Sigma-Aldrich. After thorough mixing, 0.5 grams of nitric acid (HNO_3 , 68%) was added to the combined materials in a laboratory crucible and was briefly mixed. Very quickly after mixing, another crucible would be added on top and the combination was microwaved in a standard microwave oven for 8 seconds and 12 seconds for comparison. The chemical vaporization that occurs as a result of this process produces a drastically expanded volume as the flakes expand into a low density material (Ghasemi et al., 2014). In addition, this produces a hydrophilic material due to oxidation. This material is easily reproduced for the purposes of this experiment.

2.1.2 Material Characterization

Characterization of the materials was done in two ways. First, scanning electron microscope (SEM) images were taken of the exfoliated graphite with a collection of relevant resolutions displayed. The second method was by contact angle of a drop of water on both types of exfoliated graphite (8 second and 12 second microwave exposure).

Figure 5 shows the SEM image for exfoliated graphite at 100 times resolution. A scale is shown for 100 micrometers. The expanded layers are along the “c” axis and were observed in this image. This shows the rough, porous structure of the overall structure allowing for water to pass through it easily. Figure 6 shows a much larger resolution of 10,000 times for exfoliated graphite. The image shows a layer of the graphene having been expanded in volume indicated by the streaking lines in the sample.

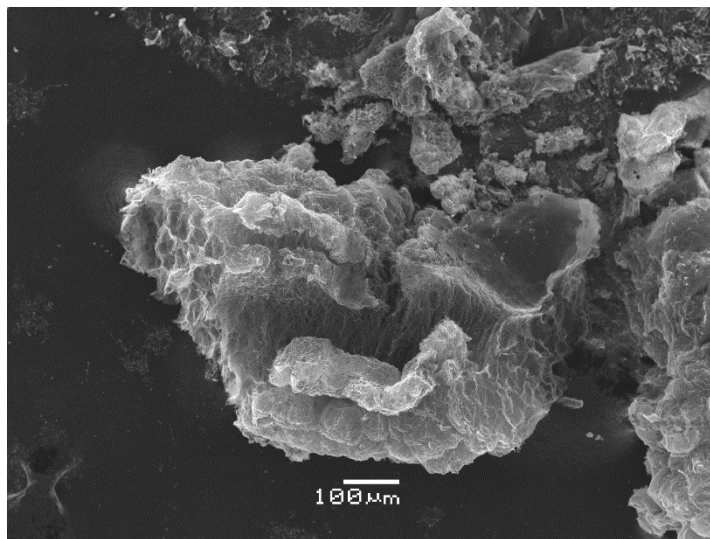


Figure 5: SEM of exfoliated graphite at x100 resolution

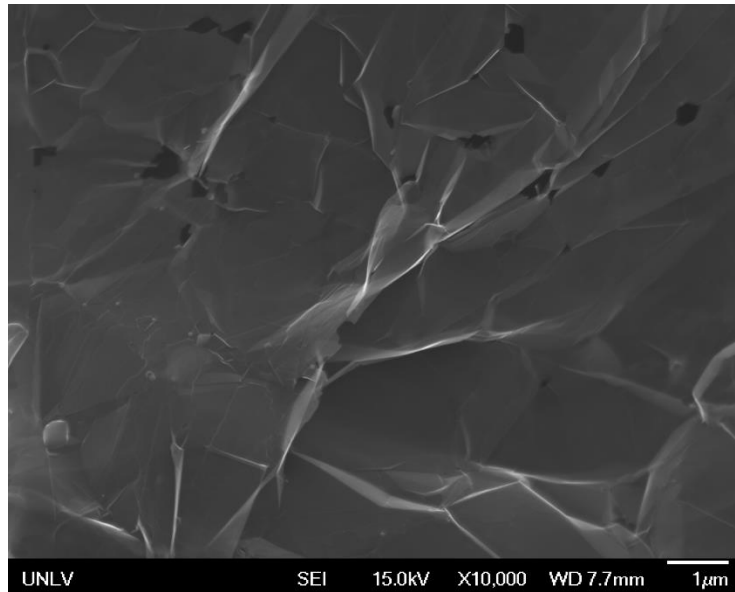


Figure 6: SEM of exfoliated graphite at x10,000 resolution

In order to evaluate the hydrophilicity of the materials, contact angles were measured with the results provided in Figure 7. It should be noted that the angle recorded is the largest one possible as with a short amount of time the water droplet saturates the material and disappears preventing continued analysis of the contact angle. The recorded maximum angle for 8 second microwave exposure is 39.05 degrees which agrees with documented sources on this particular material (Ghasemi et al., 2014). Figure 8 shows the maximum contact angle for the 12 second microwave exposed exfoliated graphite. One aspect to be observed from this image is the increased overall contact angle to 49.45 degrees. Though this material also behaves similarly with water absorbing easily into its structure, the contact angle is roughly 10 degrees larger which allows for the conclusion that the prolonged microwave emission time for the graphite produces a less hydrophilic portion in the material. The extended thermal exfoliation and microwave exposure induce the deoxygenation of exfoliated graphite which results in less hydrophilic properties (Stankovich et al., 2007; Hu et al., 2012).

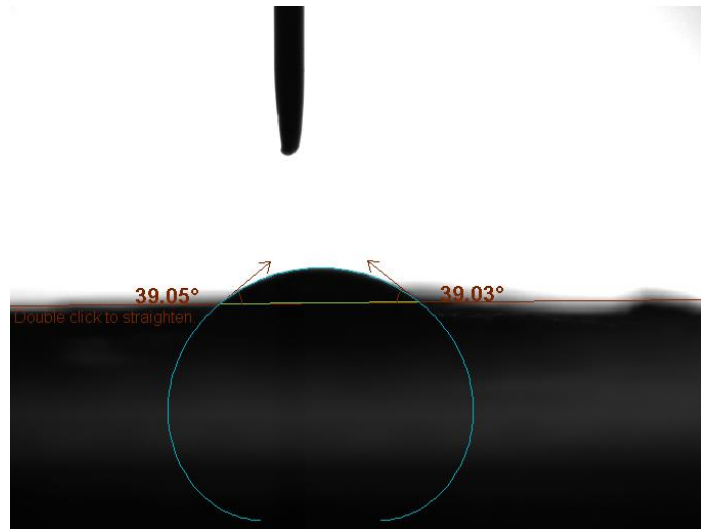


Figure 7: Contact angle for 8 second synthesis exfoliated graphite

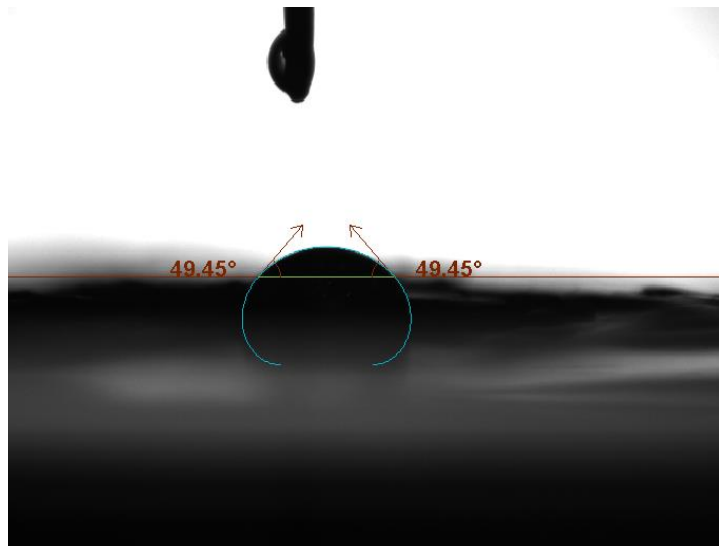


Figure 8: Contact angle for 12 second synthesis exfoliated graphite

2.2 Treated Carbon Foam

As light provides a given irradiance in W m^{-2} across a given spectrum, the exfoliated graphite absorbs it and transfers the heat to the bottom layer which is noted as the insulating layer. The insulating material has air pockets and closed pores which allow the material to float on the surface. This material is characterized as hydrophilic upon treatment which allows water to pass

through the carbon foam via capillary action. The requirements of the insulating layer are to be 1) low density to float near the surface for heat localization, 2) to be insulating in nature, and 3) to be hydrophilic for proper vapor transportation.

2.2.1 Fabrication

The carbon foam has a simpler production in that the foam base is purchased before being modified (KRR Reynolds, 80 PPI). 4% molar nitric acid is produced in a beaker with a cut piece of the carbon foam matching the desired diameter of the test chamber (roughly 2.5 inches) added into the acid and stirred for 2 hours (Ghasemi, 2014). The purpose of this treatment is to make the carbon hydrophilic like the exfoliated graphite.

2.2.2 Material Characterization

Figure 9 shows the treated carbon foam at a resolution that is only 50 times smaller. This image has some interesting properties such as the repeating hexagonal structure and the generous amount of pores that make up its several layers. The non-uniform layering represents the open and closed pores observed in previous research as a means of not only floating but allowing fluids to pass through the material.

The reason carbon foam isn't shown for contact angle is because the act of floating just below the surface demonstrates it has become hydrophilic in behavior with water able to pass through it (Ghasemi et al., 2014). Figure 10 shows a comparison of the carbon foam before acid treatment (right) and after acid treatment (left). Note the left treated carbon foam seems to sink more into the water. This is as a result of open pores being generated from acid treatment while keeping some pores closed in the material (Tsyntsarski et al., 2012). The compromise of porosity results in a beautiful combination of liquid penetration and floatation.

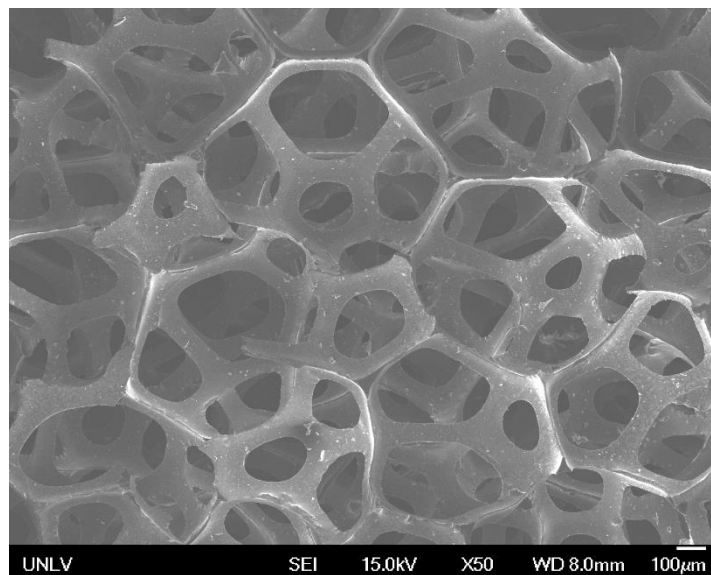


Figure 9: SEM of treated carbon foam at x50 resolution

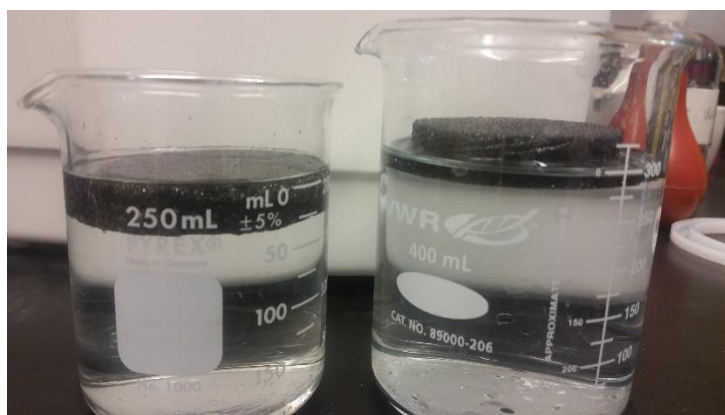


Figure 10: As purchased carbon foam (right) vs. acid treated carbon foam (left)

Chapter 3: Cost-Effective Solar Simulator

In order to perform solar distillation tests, an accurate light source is definitely required. Despite the availability of solar energy, natural sunlight proved a problem to test for this project due to the unpredictable nature of weather. A Fresnel lens mount was constructed at one point with the intent of concentrated solar power but results were challenging due to inconsistent good weather and challenges of equipment working for measurement purposes.

Many solar simulators exist today commercially with a Xenon lamp being the most relevant example as it was used in the original DLS setup (Ghasemi et al., 2014). Upon researched choices, metal halide lamps provided promising results for CSP applications (Codd et al., 2010). The spectrum, while not perfectly matched to a typical solar spectrum, does show how the lamp can mimic the overall shape of irradiance enough for low wavelength applications. Figure 11 also shows the experimental recordings compared to the shape of normal sunlight in a spectroscopy study. Though they don't match perfectly, the study is close enough for experimental purposes. The blue graph represents the data provided by the manufacturer of the lamp, PLT. The red graph is the recorded data using spectroscopy measurements. A typical solar spectrum provided by NREL is used for comparison with the metal halide data. Codd et al. designed a high concentration halide lamp for many suns, but for the sake of this project, a simple setup with less construction needs was analyzed. The goal of creating a 1 sun simulation was deemed satisfactory for analysis in order to correlate it with recorded data and add further results from there.

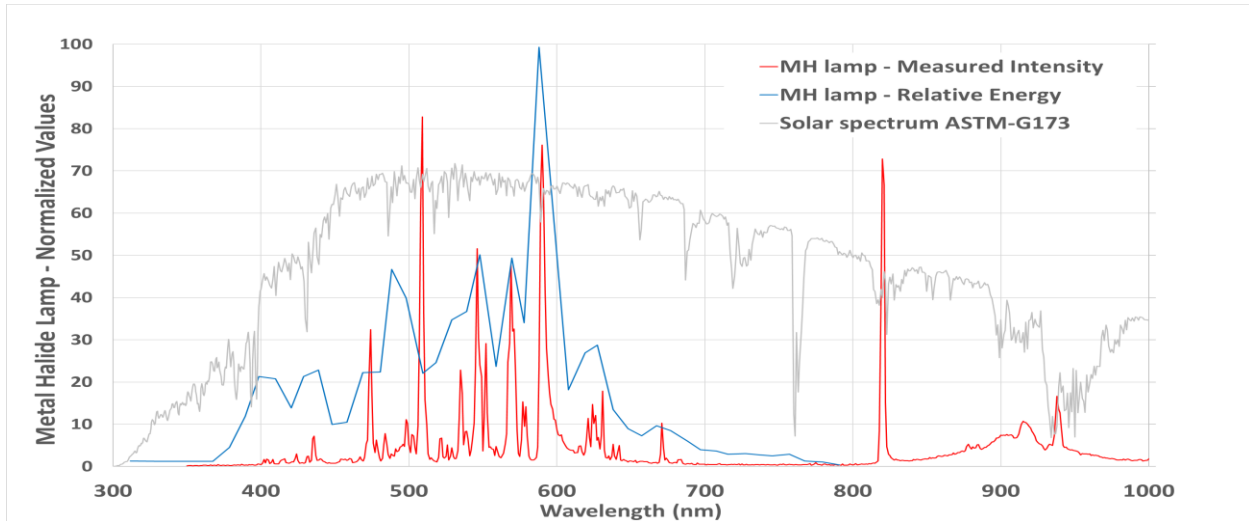


Figure 11: Modeled and recorded values for metal halide spectroscopy output compared to natural sunlight

3.1 Design Specifications

When designing the solar simulator, several factors were involved to ensure proper results:

- The setup must be able to reach at least one (1) sun intensity (equivalent to $1,000 \text{ W/m}^2$) and maintain it consistently for an extended length of time
- The setup must have as close to a solar spectrum as possible
- The lamp and other equipment must be able to function for several hours at a time over several cycles with consistent output
- The area of exposure to the solar simulator would be similar to normal sunlight as it hits a large area of the test chamber uniformly
- The equipment used for the simulated solar must be able to handle extended exposure to said heat and light

The materials used for the metal halide solar simulator were chosen based on optimal reflectivity to maximize the amount of energy transferred to the testing surface. A metal reflector designed with the 400 Watt bulbs were purchased to concentrate the light. To further improve the path of the metal halide light, a tunnel was to be developed by which the test chamber could be

elevated for higher sun exposure. This tunnel was designed with aluminum sheet metal coated with a sheet of aluminum Mylar (otherwise known as biaxially-oriented polyethylene terephthalate, or BoPET) in order to maximize the amount of light and heat reflected downward. The materials are both cheap and readily available making them great choices for a homemade solar simulator. With these parameters in mind, a general setup for simulated solar was put together that functioned for testing purposes.

3.2 FRED Simulation

The initial analysis before further experimental data was used involved simulating a general ray tracing model for how the light might behave using several assumptions to ease calculations. FRED software is an effective optical software that allows for ray tracing of many different sources whether it's solar or a lamp. Using models generated on Autodesk Inventor, an analysis involving the metal halide source and a cylindrical tunnel was conducted.

Light and radiation can be characterized using vector-based math to understand the behavior they exhibit when coming in contact with a new medium or surface. Properties like refraction, transmission, and absorption can all be described when understanding the electric field E and the intensity I as a function of the angle of attack and the initial value for each vector. Light can become polarized such that light is either transmitted or blocked from exiting a material. Intensity is described as being directly proportional to the square of the cosine of the incident angle

$$I \propto \cos^2 \theta$$

Figure 12 the model of the halide lamp recreated in Inventor and then uploaded onto FRED as a light source. The ray tracing shown is up to 100,000 rays for the theoretical study. Generally speaking, the more rays generated, the more accurate the model can be like in a finite element

analysis. The interior of the bulb containing the filament is assumed to be pure air. The enclosed bulb is modeled as a simple glass with 96% transmission and 4% reflection.

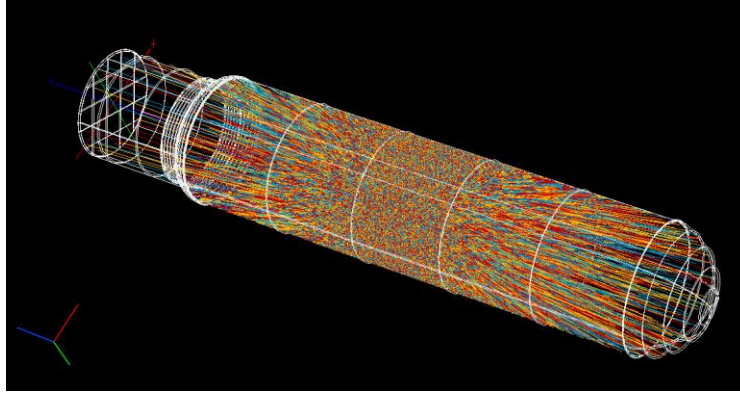


Figure 12: The source lamp with 100,000 rays being emitted

Much of this analysis relates to the basic principles of Snell's Law for light refraction:

$$\frac{\sin \theta_1}{\sin \theta_2} = \frac{v_1}{v_2} = \frac{\lambda_1}{\lambda_2} = \frac{n_2}{n_1}$$

,where n stands for the index of refraction and θ is the angle of a ray of light as it travels from one medium to another. λ is the wavelength of the incoming light with respect to the medium it is traveling through. Using further radiometry analysis, the Fresnel Equations are used to describe optical propagation.

$$R = (n_0 - n_1)^2 + k_1^2 / (n_0 + n_1)^2 + k_1^2$$

$$\varphi = \tan^{-1} \left(\frac{2n_0k_1}{n_0^2 - n_1^2 + k_1^2} \right)$$

For the variables, n and k describe imaginary and real parts of the complex reflective index \hat{N} with the connotation $\hat{N} = n + jk$, where j is the imaginary number $\sqrt{-1}$.

The reflectance for p-polarized and s-polarized light is defined by the following variables.

$$R_s = \left| \frac{(n_1 \cos \theta - n_2 \sqrt{1 - \left(\frac{n_1}{n_2} \sin \theta\right)^2}) / (n_1 \cos \theta + n_2 \sqrt{1 - \left(\frac{n_1}{n_2} \sin \theta\right)^2})}{(n_1 \cos \theta - n_2 \sqrt{1 - \left(\frac{n_1}{n_2} \sin \theta\right)^2}) / (n_1 \cos \theta + n_2 \sqrt{1 - \left(\frac{n_1}{n_2} \sin \theta\right)^2})} \right|^2$$

$$R_p = \left| \frac{(n_1 \sqrt{1 - \left(\frac{n_1}{n_2} \sin\theta\right)^2} - n_2 \cos\theta)}{(n_1 \sqrt{1 - \left(\frac{n_1}{n_2} \sin\theta\right)^2} + n_2 \cos\theta)} \right|^2$$

The measured reflectance is then taken as an average between the two values.

$$R = \frac{R_s + R_p}{2}$$

With the calculations for the reflectivity assumed, a model using our cylindrical tunnel to direct the light can be simulated. The choice of a basic cylindrical tunnel became an initial control design based on the ease of construction and predictable modeling. The material properties are not determined yet so the model is based on 100% specular reflection for modeling purposes. Figure 13 shows the result of 50,000 rays being emitted by the metal halide source. The resulting rays are reflected within the tunnel and dispersed around a target area.

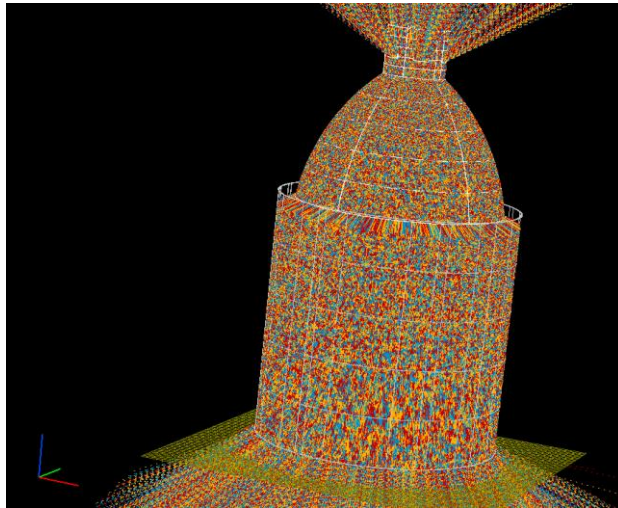


Figure 13: 50,000 Ray trace of first model for metal halide lamp with Mylar tunnel

With this simulation of ray tracing comes the benefit of modeling the physical setup before beginning construction. Figure 14 shows the irradiance distribution as a function of position with the distance from the source being 26 inches. The average output measured for the surface of the materials is 1,200 W/m² which is larger than the targeted 1 sun of 1,000 W/m². Figure 15 shows

the surface at 30 inches offset from the source which has an average recorded value of 1,100 W/m².

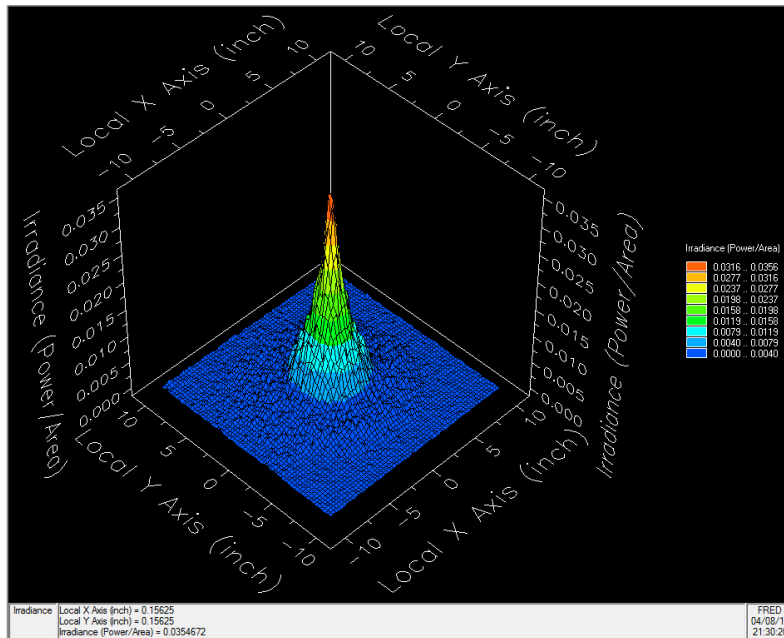


Figure 14: Irradiance spread at 26 inches from source

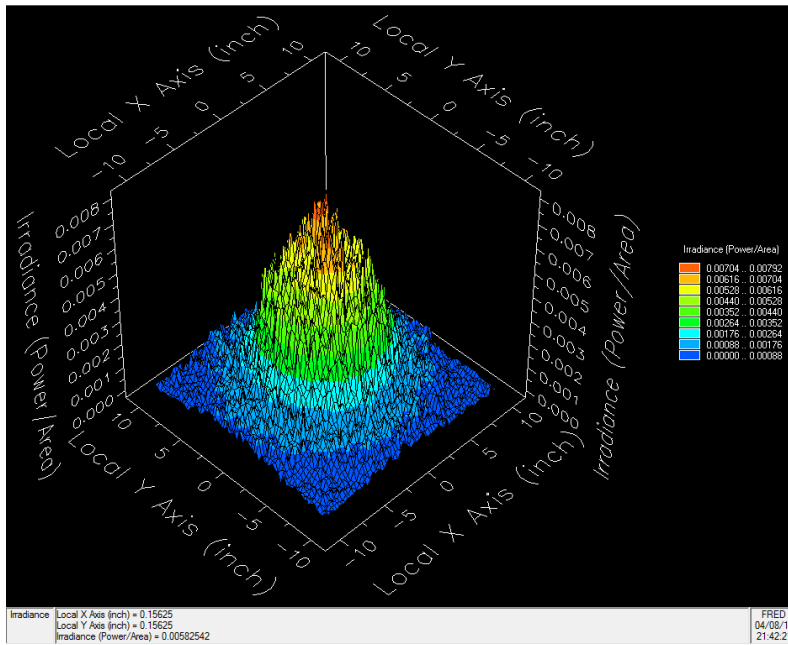


Figure 15: Irradiance spread at 30 inches from source

3.3 Experimental and Spectrometer Recordings

The metal halide lamp setup required an understanding of the wiring and the electrical properties of a ballast. The ballast and capacitor act as a means to stabilize the output of light coming from the arc within the halide lamp. Following a wiring diagram similar to Figure 16, we were able to purchase and connect the various components using wire nuts in parts to connect the ends of each cord together. Wire strippers were used to expose the connections with electrical tape used to insulate where wire nuts didn't work well. The results of connection can be seen in Figure 17 with the metal halide lamp showing an emittance of light.

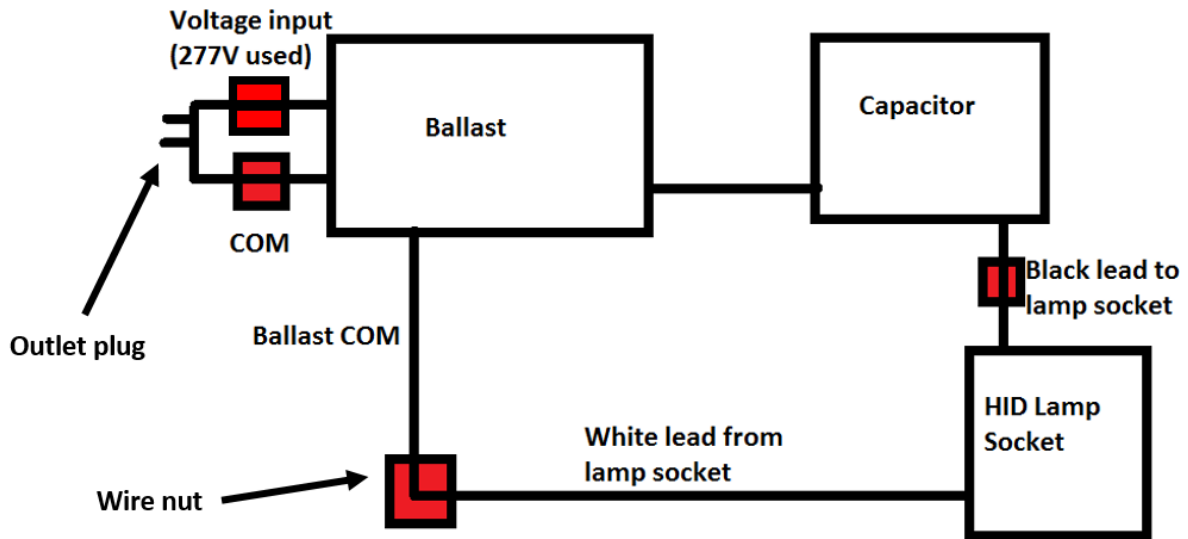


Figure 16: Ballast wiring diagram for metal halide lamp

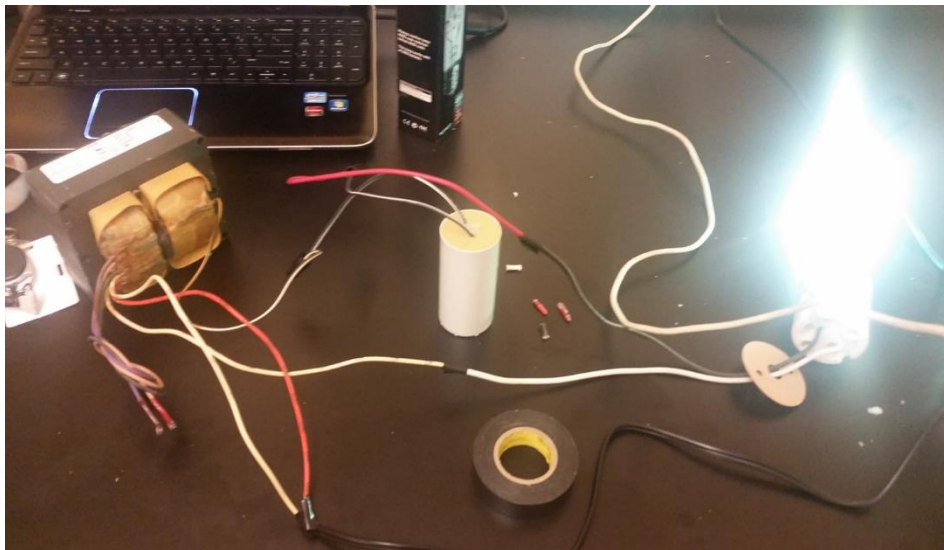


Figure 17: The physical working wiring for the HID setup



Figure 18: The metal halide simulated solar basic setup

Mylar was applied to the inner surface of the aluminum sheet metal that was shaped into a cylinder using duct tape for a secure hold. The Mylar tunnel was attached to the reflector which hangs on the socket of the metal halide lamp. Figure 19 shows a view of the Mylar as it hangs on the surface of the aluminum sheet metal.



Figure 19: Aluminum hollow cylinder with Mylar coating around inner surface

As the solar simulator was built to the desired structure, some features were noticed while measuring irradiance with a pyranometer. The output of the metal halide lamp seemed to give more optimal numbers with a slight tilt in angle suggesting the model should be updated to reflect this. Measuring the new angles in Figure 20 told us the tilt after correcting for the reflector and Mylar tunnel should be 12.94 degrees. Figure 21 shows the resulting adjustment to the Inventor model.

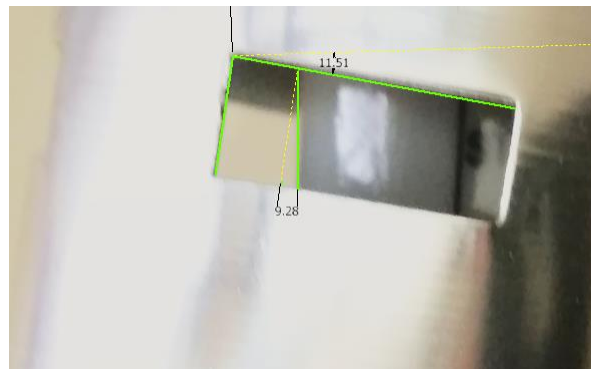


Figure 20: Measurement of angular offset for reflector and Mylar tunnel

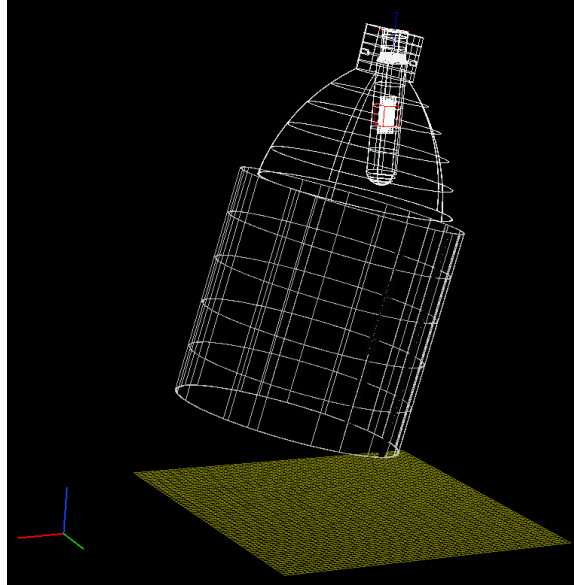


Figure 21: 12.94 degree adjustment of bulb with reflector

The model was then simulated again for the more current setup in order to see what kind of numbers are obtained for the optimal position under the Mylar tunnel. Figure 22 shows the ray

trace at 50,000 rays for a more time-consuming but accurate result before moving forward into testing.

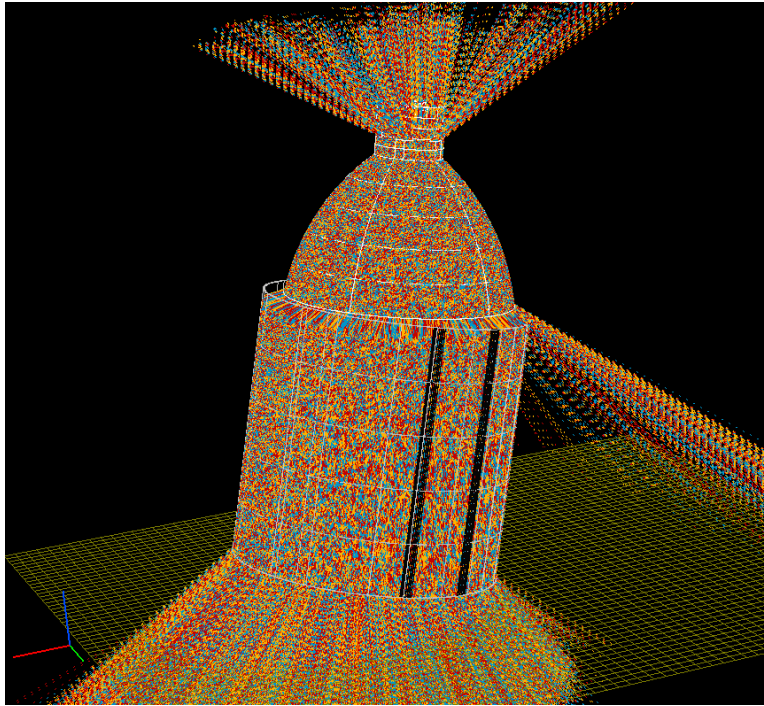


Figure 22: Ray trace of 50,000 rays of adjusted source

Figure 23 shows the new output for irradiance and the optimal position for maximum energy exposure at 26 inches from the source. The optimal position along the x and y axis is also shown in Figure 24. From the center, the coordinates of (0.3125, 5.9375) are where the most irradiance is being emitted.

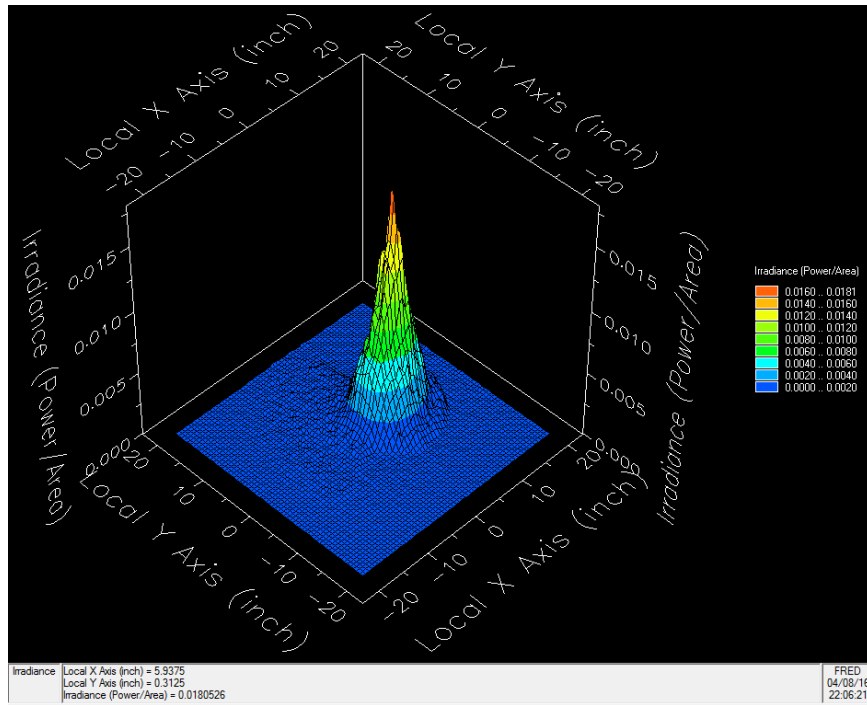


Figure 23: Irradiance of adjusted source at 26 inches

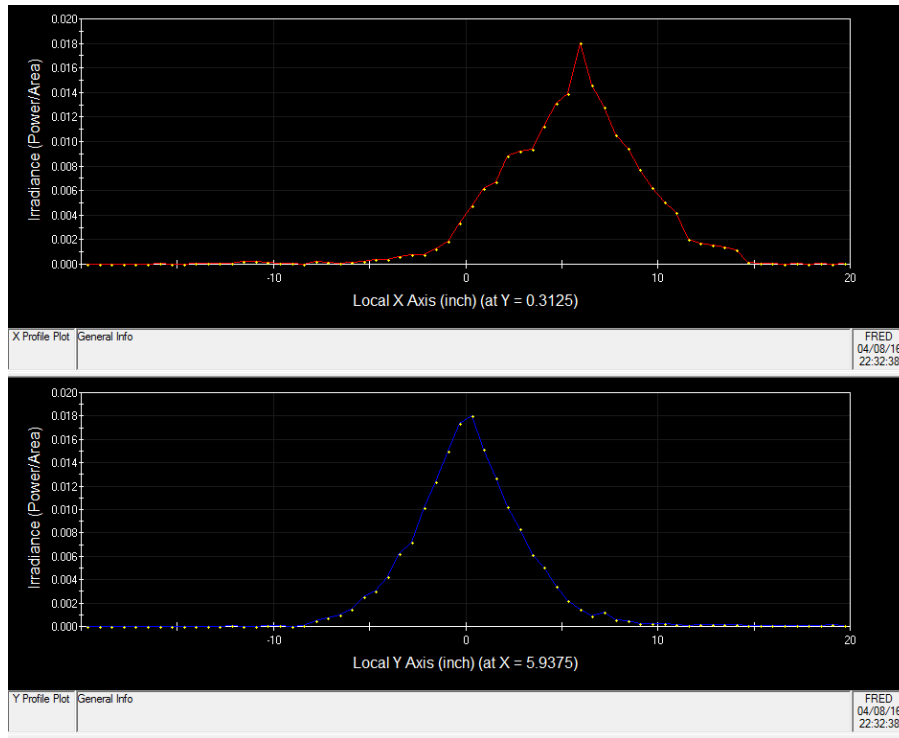


Figure 24: Maximum positioning for the irradiance model at 26 inches offset

As the study continued, a more meaningful measure of the material properties was conducted using a spectrometer to measure intensity at the various wavelengths. This not only would allow for a more accurate recording of reflectance but also for a proper reading of the metal halide's spectrum. The lamp was measured for several angles as well as for how the light measured when bounced off a reflective surface used in the setup. Using an Ocean Optics spectrometer and special fiber optics, the metal halide lamp's intensity was recorded and analyzed on Excel.

The final results after adjusting the model to match the most accurate version of the metal halide source is displayed in Figure 25. The average irradiance is calculated as $1,373 \text{ W/m}^2$. This allows the conclusion that the testing surface is reaching one sun for testing purposes. The area is also narrowed down to within the testing surface. The final positioning for the peak concentration of irradiance is shown in Figure 26.

It is important to note that there are small peaks in the irradiance data approach $7,800 \text{ W/m}^2$ with other high values beyond one sun. This is due to the smaller converging setup of light compared to the plane wave nature of natural sunlight. The energy output provided is what's important for this study with further analysis going beyond the scope of this project. Previous studies have been done that have used metal halide lamps as a solar simulator despite its limitations and so that research justifies its use in terms of relative energy and the actual response of the experimental setup.

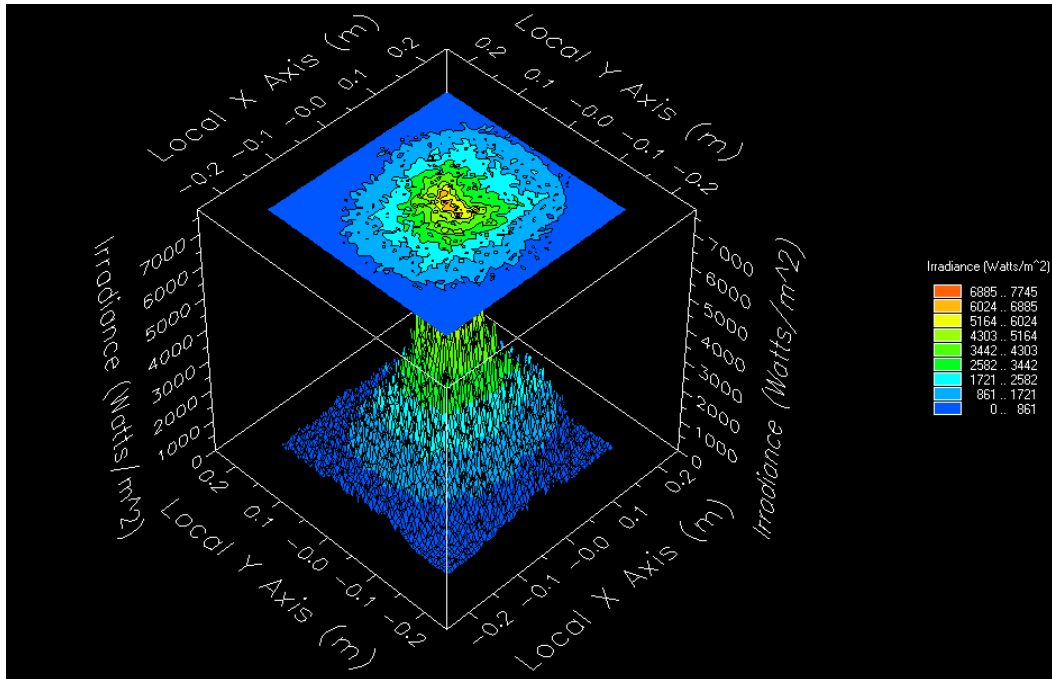


Figure 25: Final irradiance distribution of experimental metal halide source

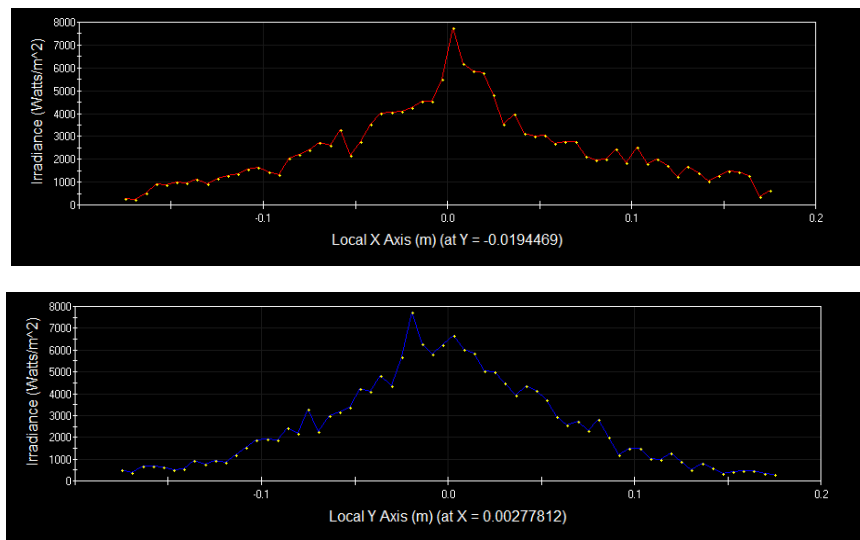


Figure 26: Final x and y coordinates from center of lamp for optimal metal halide exposure

Chapter 4: Water Evaporation Efficiency

It's important the DLS performs as reported in previous sources so the experimental setup is crucial to be close enough to see an improvement in overall evaporation rate. The setup is essentially three main parts combined into a working process.

The first component is the test chamber with a hollow center that has another chamber within that is hollow such that water can be placed inside for testing. The outer hollow section of the chamber is filled with hydrophobic aerogel that provides thermal insulation. The material that makes up the test chamber was purchased from Port Plastics and is classified as a Polyetherimide based polymer (also known commercially as Tecapei) that was chosen for its good thermal and physical stability under heated conditions. The second component is the experimental equipment. This includes a mass balance (purchased from Adam Equipment), a National Instruments Data Acquisition device (DAQ) with thermocouples on the test chamber, the pyranometer and multimeter, and the laptop used with LabVIEW to measure the important values of the project which include mass change, temperature distribution, and the output irradiance of the lamp source. The mass balance and DAQ are connected via USB to the laptop providing a reliable connection for data acquisition. The third component is the metal halide lamp with the aluminum reflector tunnel. A basic wiring is set up to provide power to a metal halide lamp that consist of a ballast, a capacitor, a socket, and a basic outlet cable.

As mentioned in chapter 1, the thermal efficiency of the mass change caused by the DLS is calculated by using the following equation:

$$\eta_{th} = \frac{\dot{m}h_{LV}}{C_{opt}q_i}$$

The \dot{m} represents mass change, h_{LV} is the total enthalpy of the phase change for the liquid-vapor phase (2,257 kJ/kg), C_{opt} represents the optical concentration (1 for 1 sun), and q_i is the nominal input irradiance (1,000 W/m²).

4.1 Design Specifications

For the design of the experimental setup, more important specifications were kept in mind:

- The equipment must be able to communicate with computer software (specifically LabVIEW)
- The data obtained for temperature must be obtained for varying depth in order to measure the difference in temperature between the surface and the bulk water
- The mass balance must be able to record change in mass over extended periods of time
- The setup must in some way be portable enough for shifting to different locations whether it's outdoors for natural sunlight or indoors for simulated solar
- The LabVIEW programming must be able to work independently and consistently to record values over time and output the results into readable files
- The test chamber must be well insulated to prevent heat loss
- The equipment must be able to handle recording many different setups throughout the time of the project

Under these conditions, a basic design was made for obtaining the experimental results needed to determine the efficiency of the DLS distillation.

4.4 Experimental Procedure

The development of the experimental setup started with acquiring the material for the test chamber. The polyetherimide material (provided by Port Plastics) used for insulating the setup was bought as a large cylinder that was later cut using a machine shop in order to form two

concentric chambers that would be laid on top of one another. The outer chamber measures at 100 mm and holds the smaller 50 mm chamber along with hydrophobic aerogel particles (provided by Aerogel Technologies) being used as insulation between the gaps of the two chambers. A lid was fashioned out of the remaining material and the entire chamber was sealed with duct tape with the inner chamber exposed. This would be the empty volume used for water testing.

The mass measuring equipment was a USB-compatible mass balance obtained from Adam Equipment. The maximum weight was scaled to 3,000 grams with 0.1 gram incremental readings. The electronic balance can communicate with a computer to record values and allows for continuous readings. The USB cord is connected to the mass balance and laptop followed by turning on the mass balance, adjusting the settings for a serial connection before the balance finishes starting up, saving the settings, and allowing the balance to finish calibrating. In LabVIEW, the Measurement and Automation Explorer is used to make sure a secure connection has been established where the values being sent from the balance correspond with the settings on the computer for communication.

The temperature was measured using a National Instruments DAQ device. By using an electric welder, T-type thermocouples were prepared by welding one end of the cords together after stripping the wire to expose the metals. The other end was inserted into the DAQ at the appropriate channels (1 through 6) using a precision screwdriver to connect them to the hardware at the positive and negative inputs. The thermocouples are then secured using scotch tape along the inside of the test chamber in increments of roughly 10 mm in order to see the change in temperature of the bulk water compared to the generated steam surface. The DAQ is connected to a laptop via USB much like the mass balance.

The multimeter used to measure Voltage was set to DC inputs for 100 mV readings on the front interface. Two banana connectors were used to connect two wires to the multimeter's positive and negative ends that lead to a pyranometer provided by Eko Instruments used to measure irradiance from the solar source. Voltage can be converted to irradiance using a simple equation relationship between the output voltage and the sensitivity value for the pyranometer:

$$I = \frac{E}{S}$$

, where I is measured in Watts per meter squared, E is measured as microvolts, and sensitivity is measured as microvolts per Watt per meter squared. The result is measured as mV so converting the output E value to microvolts by multiplying by 1,000 gives an accurate value for irradiance. For example, to obtain one sun recordings, 8.85 mV had to be read because the sensitivity value is defined as 8.85 for this particular pyranometer.

With the experimental equipment set up in such a way that the test chamber and mass balance are under the solar simulator with the thermocouple attached, testing can be conducted. 200 mL of various quality of water have been measured and added to the test chamber before adding the prepared nanocomposite to the surface of the water (depending on the testing configuration). The nanomaterials float in the water and the lamp is turned on allowing roughly 8 minutes to start up before placing the pyranometer under the solar simulator to estimate the irradiance being generated. The pyranometer is raised using a lab jack to get an exact height while being adjusted under the lamp for a 1 sun measurement of 8.85 mV on the multimeter. Once an optimal position is confirmed, the test chamber is moved in place of the pyranometer under the lamp and raised up using lab jacks to begin testing. The LabVIEW programs are run and a period of approximately 2 hours is used to allow the setup to record results.

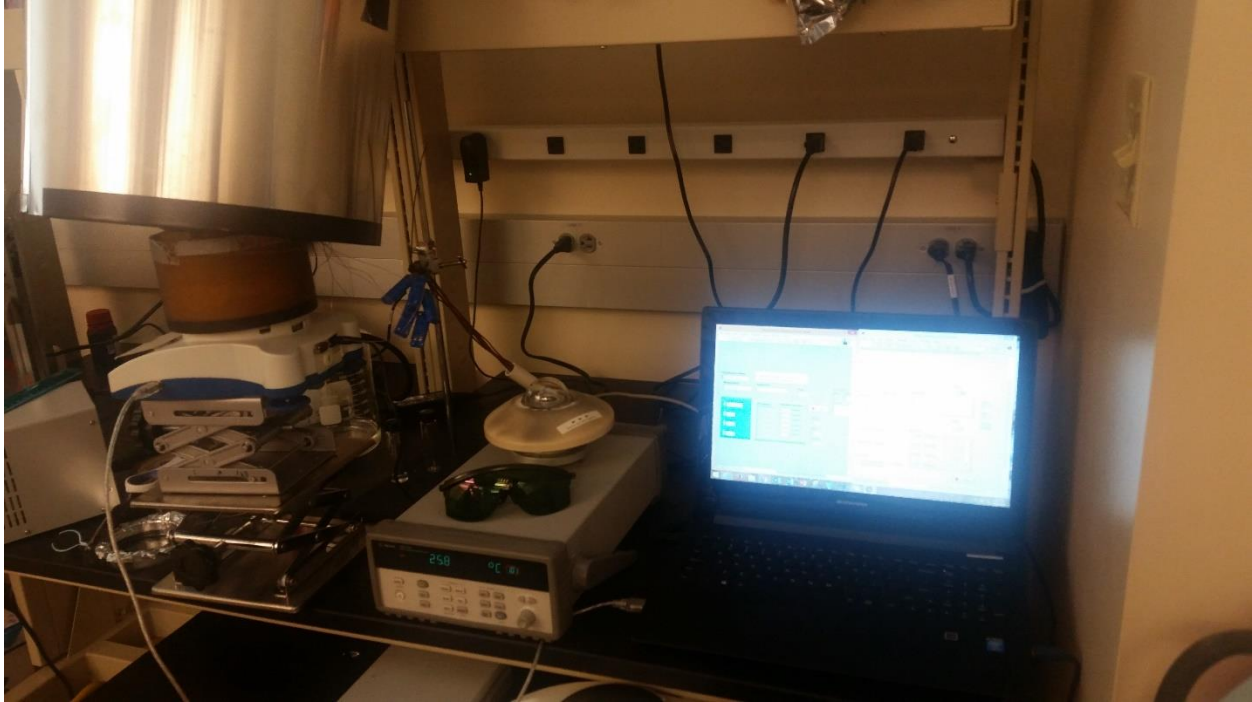


Figure 27: The full experimental setup ready for testing

4.2 LabVIEW Programming

The LabVIEW programming was broken into two VI's: the first program records mass from the mass balance via USB with a VISA program and the second records temperature from the DAQ using the thermocouples as a recording instrument. Both programs can work simultaneously and also record the time until the program is stopped and the text files are saved. Occasionally, due to errors on buffering, the mass program may fail but the file itself can still be saved with the time known when the program stopped. The VIs were built using existing modules within LabVIEW that were modified to fit the desired need of the project for mass and temperature recording. The exact design for the programs are shown in the Appendix section.

4.3 Heat Transfer Modeling

In order to understand the heat loss associated with the proposed setup, an analysis on Autodesk's Simulator Mechanical software was completed. The goal was to associate all heat transfer with the material properties of this experimental setup.

Table 2 shows the properties that were used in the heat transfer modeling. The values reflect researched values that correlate with both with vendor material sheets and further researched values. The measurement of thermal properties, while not incorporated directly in this analysis, was experimentally tested in a previous study in order to determine the conduction through the carbon foam and exfoliated graphite (Ghasemi et al., 2014). This allowed for a simplified analysis as the materials are porous when evaluated in the study while the simulation for this project can be done using bulk materials.

Table 2: Material properties for experimental setup

Material Property Reference Sheet			
Material	Specific Heat	Density	Thermal Conductivity
	J/kg*K	kg/m³	W/m*K
Exfoliated Graphite	830	0.015	0.93
Carbon Foam	1260	0.0426	0.43
Tecapei	2	1270	0.216
Aerogel	0.84	180	0.12
Water	4186	1000	0.6

Note: Data for material properties was gathered from Engineering Toolbox (2016), Aerogel Technologies (2016), KRReynolds (2016), Ghasemi (2014), Chugh (2002), and Celzard (2005).

The results are shown using Autodesk Simulation Mechanical for a basic heat transfer analysis. A convective air boundary condition of 50 degrees C and a heat source across the material surface of the setup of 1,000 W/m² (a 1 sun estimate on irradiance) was used for analysis. The simulation was run for steady state conditions in order to see optimally how setup responds

under an extensive amount of time under the sun. The chamber is shown in with a clear temperature distribution. The temperature peaks at the surface of the absorbing layer while the water temperature remains lower thanks to the insulating layer to generate a gradient. The test chamber's insulating properties make sure the heat loss is minimized over an extended period of time. A peak temperature of 106.7 degrees Celsius is achieved near the top of the DLS while a lower temperature of approximately 69 degrees Celsius is maintained in the lower bulk water. The values reflect the heat localization effect the DLS has on the water as the temperature gradient remains regardless of the amount of energy being applied to the nanomaterials.

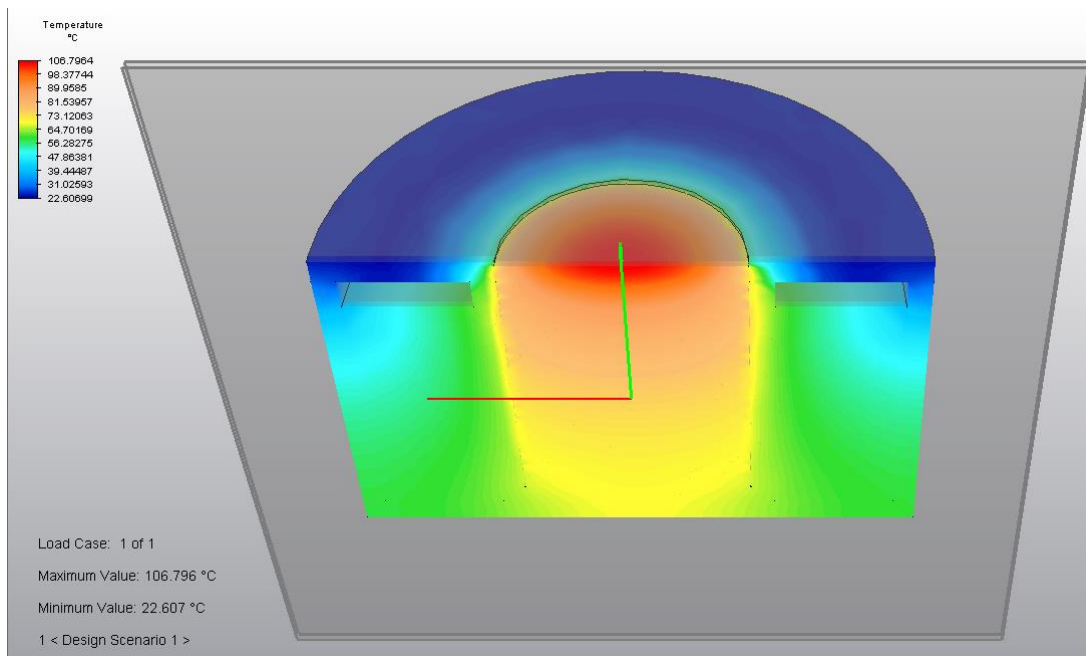


Figure 28: Autodesk Simulation Mechanical temperature distribution

4.5 Results and Discussion

The results from the mass change recordings on LabVIEW are displayed in the following figures. Figure 29 shows the mass change with a one sun measurement comparing water alone, exfoliated graphite in water, carbon foam in water, and most importantly the DLS in water. The dramatic slope of the DLS graph demonstrates the improvement heat localization provides as the

water is steamed quickly due to the material’s properties. It is worth noting that the small differentials in the data are a result of slight motion and vibrations of the setup. The slope does maintain a consistent appearance despite these brief lapse in recording.

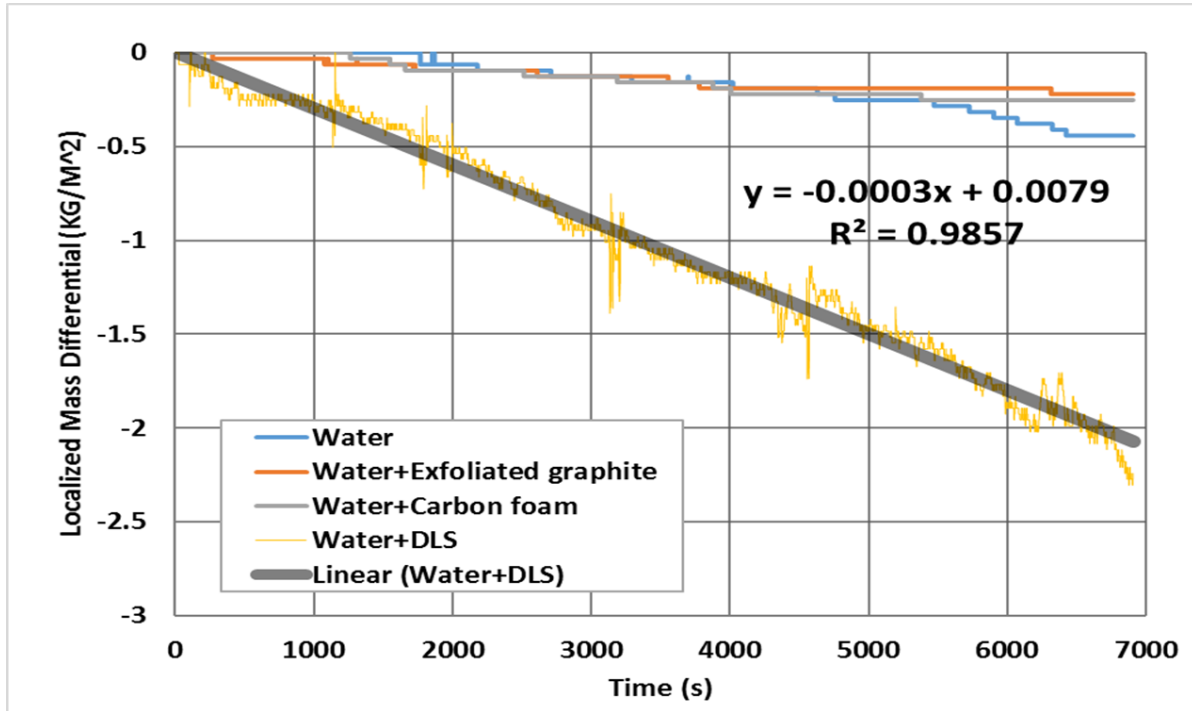


Figure 29: Results for 1 sun testing

Table 3 shows the tabulated results of the evaporation rates with the efficiency being calculated for each test setup. Using the thermal efficiency equation, the results show that the nanomaterials individually seem to do worse than water alone. This could be because the exfoliated graphite absorbs the heat from the solar simulator and transfers it directly to the bulk water which, due to water’s high heat capacity, distributes and doesn’t result in successful steam generation. The carbon foam, insulating the heat in place, seems to do slightly better than the graphite but only due to the heat localization it provides. The lack of further absorption provided by the DLS makes for a less efficient setup. The DLS does much better than the rest of the tests demonstrating its very clear advantages with a 39.3% increase in efficiency based on calculations.

Table 3: 1 sun mass change recordings

1 Sun Mass Change Efficiency Measurements		
Testing Setup	Mass rate change (kg/m ² *h)	Efficiency
Water	0.241	11.2%
Water + Exfoliated Graphite	0.115	5.4%
Water + Carbon Foam	0.163	7.6%
Water + DLS	1.084	50.5%

An important aspect to the entire goal of heat localization with this project is a temperature differential. If there is heat localization, then the heat flux generated from the solar simulator can generate steam that much quicker. Each test situation was measured for temperature with first results shown with water alone in Figure 30. Sometime the thermocouples may not work for the entire test due to how sensitive they are so some were either filtered down or are left as they are because the result is still clear. For water alone, the temperature seems to be gathering towards a steady state temperature with little to no temperature difference. This indicates that the entire volume of water is absorbing the lamp closely such that the heat is dispersed and water vapor is not easily generated.

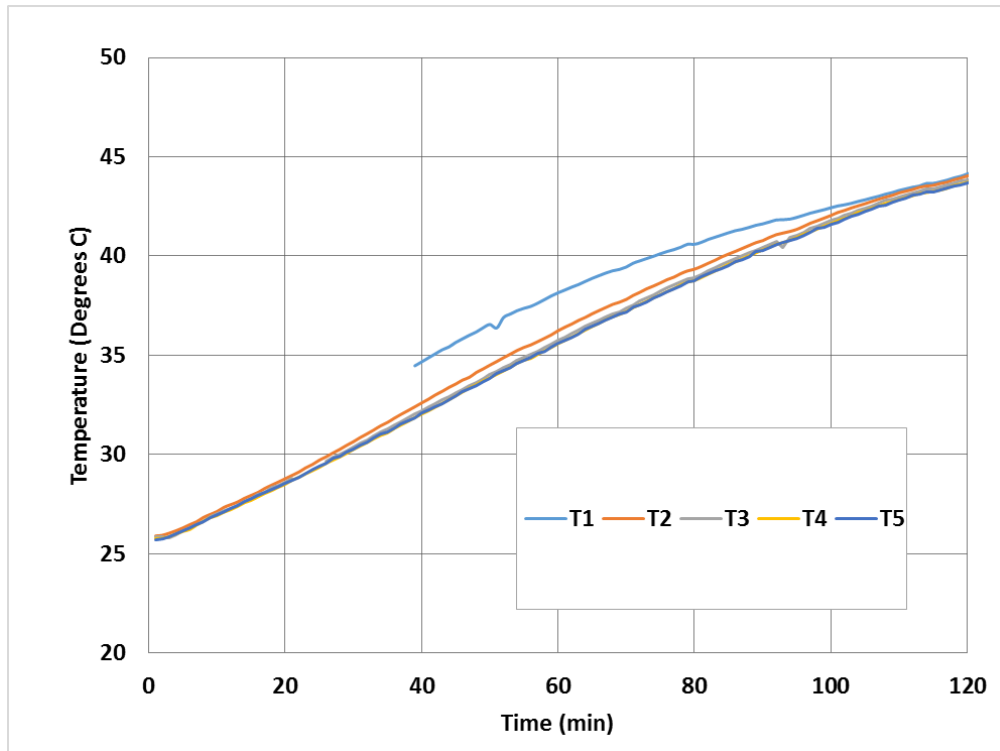


Figure 30: Result for 1 sun water alone temperature distribution

Figure 31 shows the effect exfoliated graphite is having on the water. Although there is a temperature gradient, the water seems to be increasing at the same rate and thus the heat transfer seems to stagnate as the graphite absorbs the solar energy at a fast rate but with little improvement. Some error measurements occur here that make interpreting the graphs challenging but the overall takeaway is the temperature difference is not very high. As for Figure 32, the carbon foam alone doesn't seem to improve the heat transfer process as the heat is both slowly absorbed and then slowly dissipated into the water over time. The temperature gradient is there (despite the cutting of bad data for the first thermocouple), but it's a very small difference. The lack of heat flux the exfoliated graphite provides creates a consistent equilibrium on temperature between the water and the carbon foam.

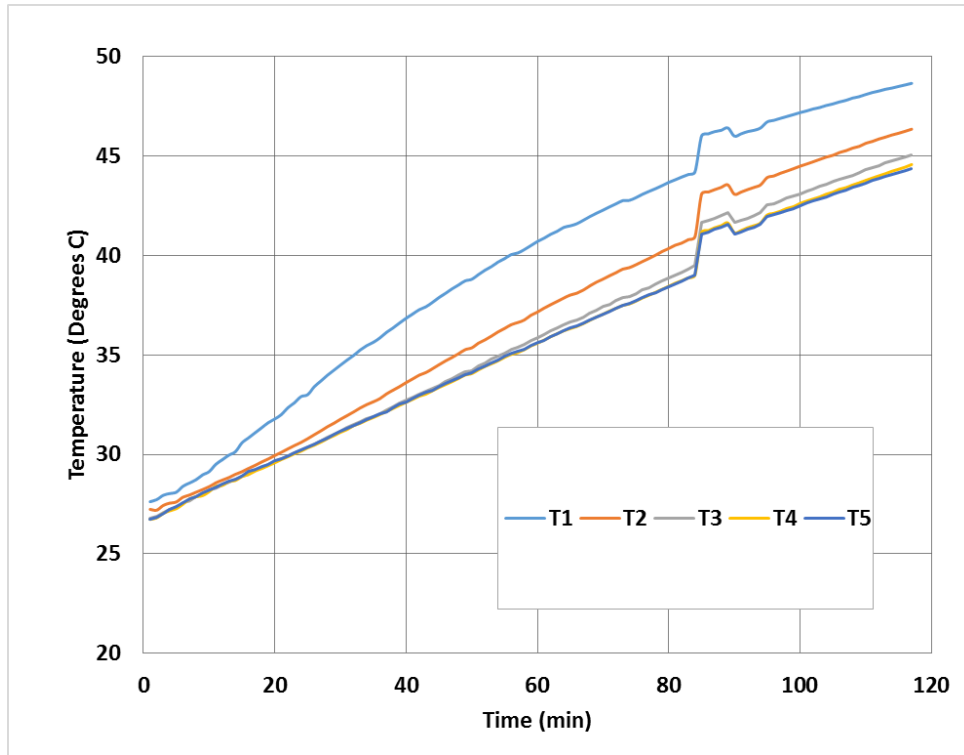


Figure 31: Result for 1 sun exfoliated graphite temperature distribution

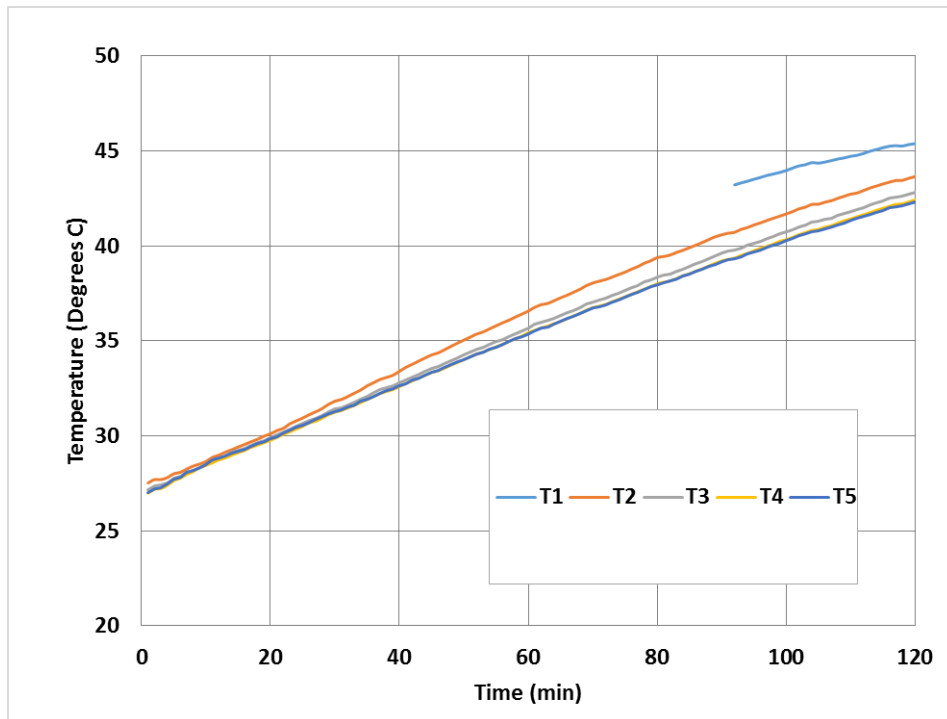


Figure 32: Result for 1 sun carbon foam temperature distribution

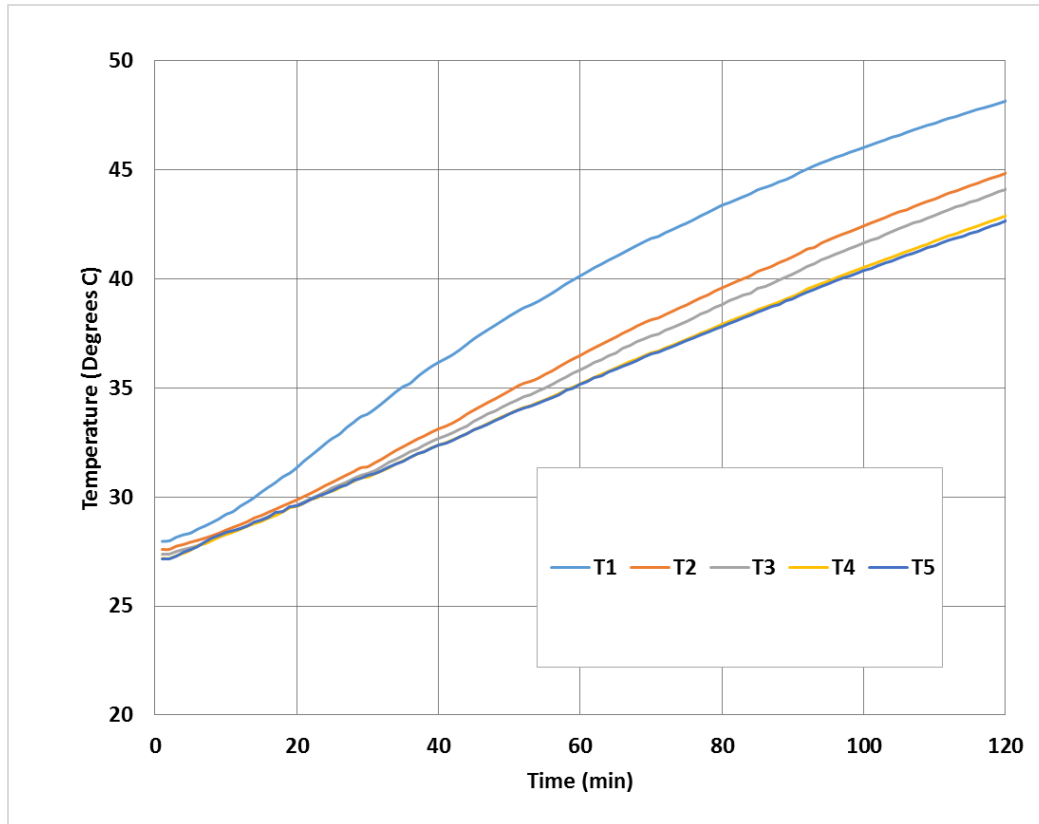


Figure 33: Result for 1 sun DLS temperature distribution

Finally, we can see in Figure 33 the effect of both nanomaterials incorporated together as they help generate steam in tandem. The temperature gradient is strongest in this setup with an approximate 6 degree difference that facilitates heat transfer better than any other setup. As this is the best indicator of the DLS serving its purpose with the mass change, the theory of heat localization causing increased steam generation is reinforced.

Chapter 5: Water Purification

In order to evaluate the suitability of the solar distillation process with heat localization suggested in this research, water quality verification was conducted. The quality of purified water from the solar distillation process with the DLS was evaluated. Water distillation quality was evaluated using Horiba's Aqualog measurement hardware. The equipment uses fluorescence excitation-emission procedures to produce fluorescence spectra that are recorded to evaluate the

response as the instrument analyzes a water sample. A UV-VIS spectroscopy study was also used. More details about the hardware and software will be discussed.

5.1 Aqualog Hardware and Software

The setup for the Aqualog works as part of software that uses Matlab coding to analyze samples across a range of wavelengths. It uses a xenon-arc light source to provide a means of UV-absorption to see if colored dissolved organic matter (CDOM) exist within a sample. A quartz cuvette is filled with a water sample and is then placed into the machine where the fluorescence procedure takes place. The first 3 samples are described as Raman samples. These tests are to show where a color intensity and where a variation in chemical composition might exist. The Raman samples are taken so as to be removed when looking at the final results as they correlate to pure water's properties rather than the contaminants. An EEM test is done that will produce a graph of varying intensity for excitation and emission that shows where contaminants exist in the water sample. Removal of "inner filter effects" (IFEs) and Rayleigh scattering is also done to correct data generated during the analysis much like the Raman scattering. A sample with a low intensity reading throughout the measured spectrum (a consistent dark blue hue) is deemed a clean sample for the purposes of this study. In the context of this study, the original water sample would remain consistently clean of organic samples with no new excitation peaks occurring throughout the sample.

5.2 Fluorescence and UV-VIS Spectroscopy

Two tests are conducted in order to characterize the extent of water purification. These tests are known as fluorescence and UV-Vis absorbance. Fluorescence is a means of looking at the excited state caused from the process that results in a photon being emitted to return to a stable ground state. As discussed previously, the EEM results show the reaction a sample has from being

excited by fluorescence. When UV-VIS spectroscopy is used, a material is exposed to electromagnetic energy and light is emitted by particles in that material that is a result of absorbing that energy. This can be measured with a wavelength characterization that corresponds to different intensities. Both tests are used to determine contaminants that are in the water samples collected. The science of this process is helpful for this project and will be examined for the distilled water that was successfully collected in this project. A sample that had been contaminated with potassium permanganate, an inorganic, was tested as it easily dissolves in water with a distinct color. Seeing how the water changes before and after treatment is of interest.

5.3 Results and Discussion

Using a small-scale water collector like in Figure 34 to distill and collect water, results were analyzed using the stated fluorescence and absorbance tests. The water collector is based on a single slope solar still but has been minimized in order to facilitate saturation on the glass surface. After the evaporation and condensation process has completed, the water was collected using a compressed air gun to gather any remaining water together that was on the glass surface and was placed in a vial for testing. The results took approximately are shown in Figure 35 with 5 hours to collect which could be because of escaping vapor and the challenge of a high temperature surface on the glass.



Figure 34: Distilled water on water collector

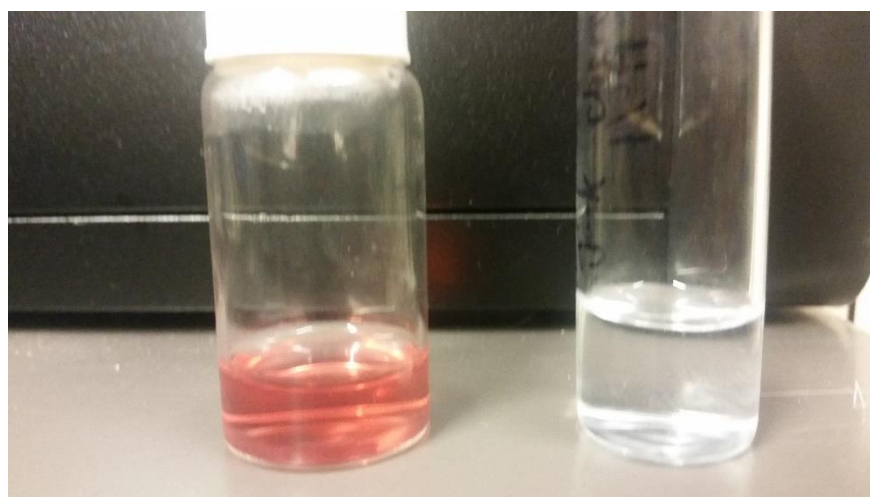


Figure 35: Contaminated potassium permanganate water (left) and final distilled water (right)

Figure 36 shows the water sample before testing for fluorescence. The water was very clean tap water spiked with potassium permanganate that would act as a good control to see if the water remains as clean. As Figure 37 shows, this was not the case. The water that resulted from this process seems to have gotten slightly contaminated the samples with a material in the 350 nm range on the spectrum with some smaller contaminants in the 250-300 nm range. Due to the unstable nature of distillation, many possible candidates could have been easily picked up in water vapor as it evaporated and condensed. Contaminants in the air, on the surface of the glass, within the solar basin, or from the carbon DLS itself could have easily been carried into the water sample.

Unfortunately, based on consultation of similar graphs and other peers, the results are uncertain as to what was carried into the water. Despite careful setup to ensure as few contaminants as possible, there is potential the water was exposed in some way to outside contaminants. It should be noted that similar results were obtained twice for these graphs when testing with just tap water. A more professionally designed solar still that is well sealed and possibly vacuumed would avoid this problem.

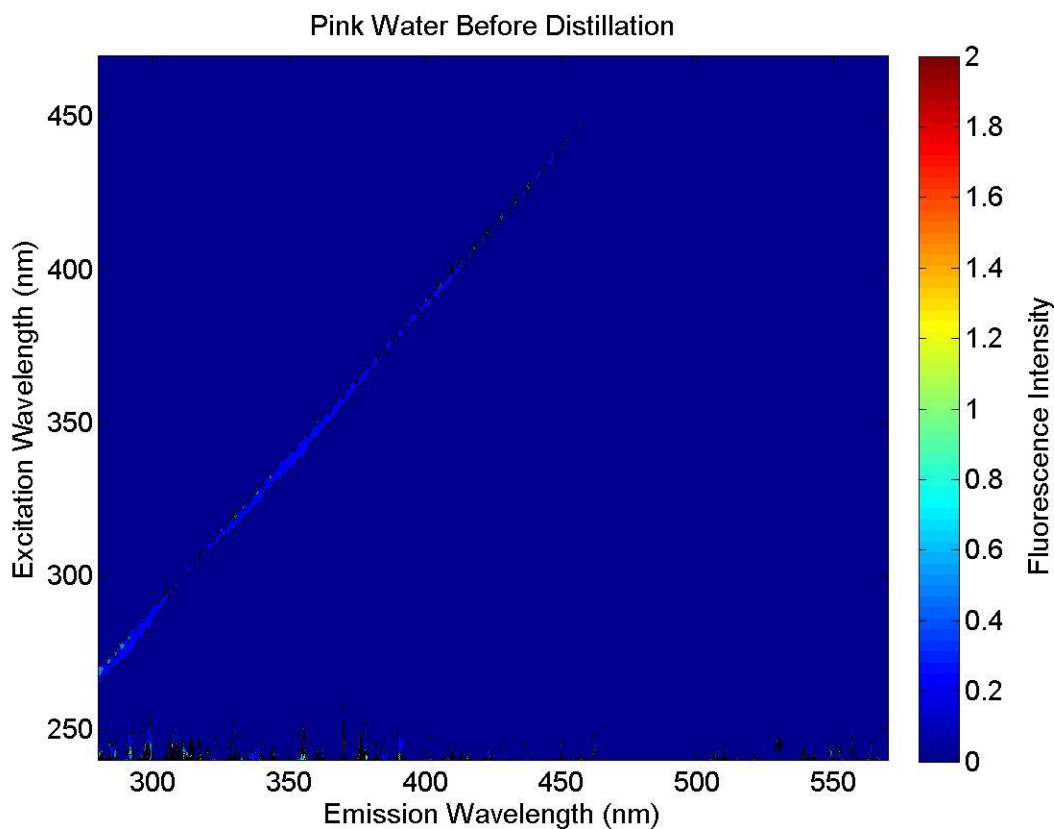


Figure 36: Initial EEM of potassium permanganate water in fluorescence

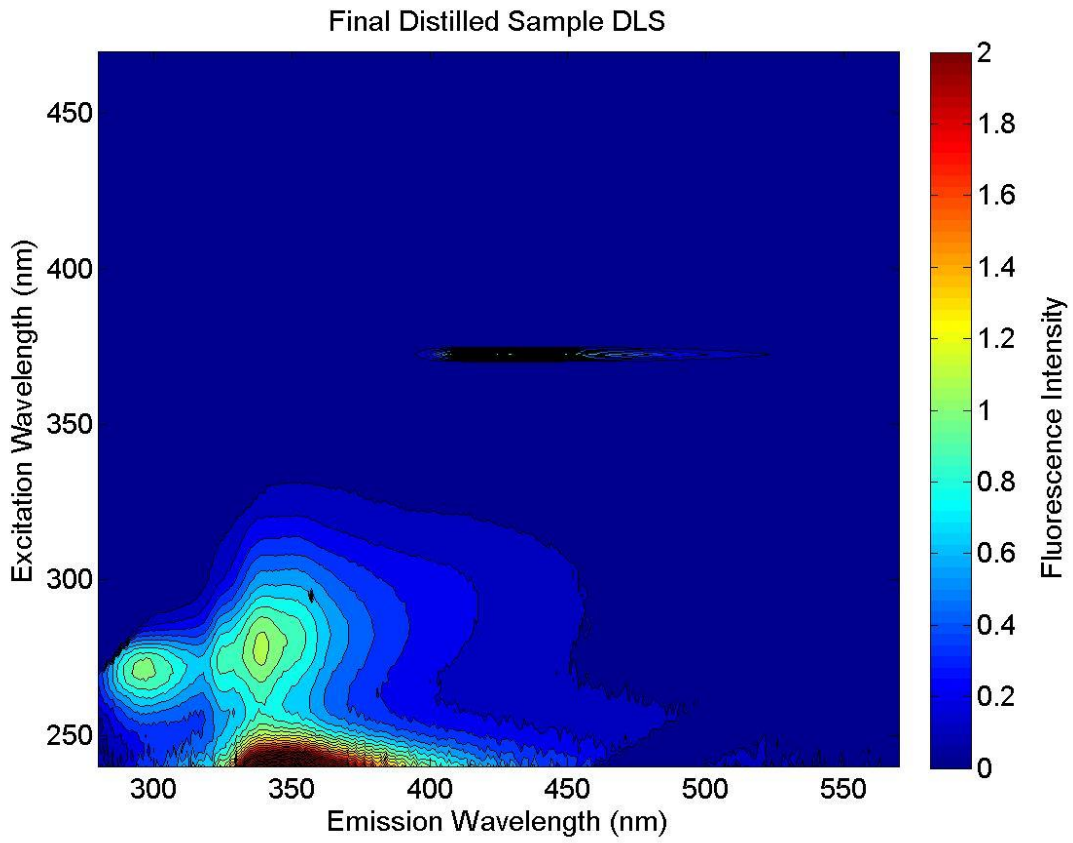


Figure 37: Result for EEM of distilled water from setup in fluorescence

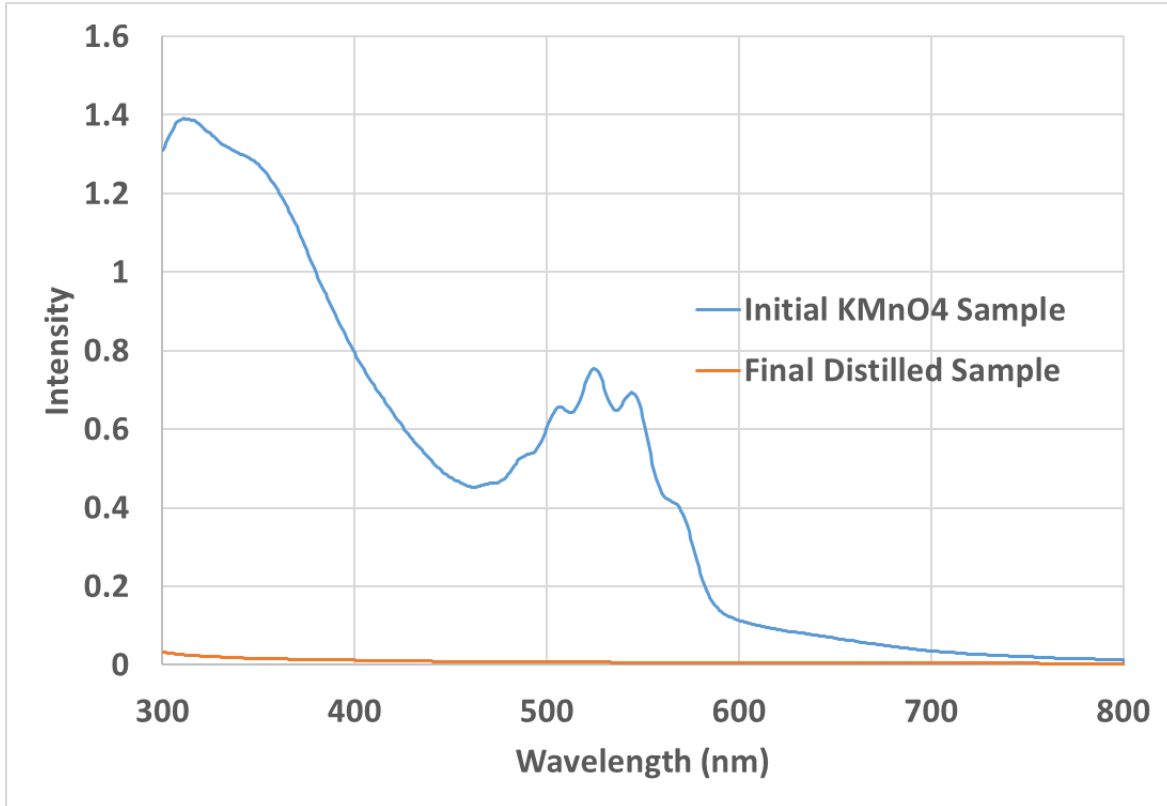


Figure 38: Result for UV-VIS Spectroscopy of Potassium Permanganate distillation

From the UV-VIS spectrometer testing, Figure 38 shows the results of the cleaning of potassium permanganate. The blue graph represents the inorganic material with some slight variation due to decomposition. The orange graph plainly states that the distilled water is free of the potassium permanganate from the distillation process.

Chapter 6: Conclusions and Future Work

6.1 Conclusions

The final results for the DLS nanomaterials combined with the metal halide solar simulator show positive correlations on the mass change and temperature recordings.

The exfoliated graphite and carbon foam nanomaterials fulfilled their purpose and demonstrated their desirable properties for heat transfer and allowing water to pass through their structures. The easily obtainable materials have great application for solar distillation and show promising results both for steam generation and water purification.

The metal halide solar simulator proved fairly accurate both in model and experimental results for the project's purposes and was very helpful for laboratory environment testing. The relative low cost and simple design lend themselves to easy replication in order to complete further testing on not only this study but other studies involving solar power when weather can be an issue in specific regions.

The heat localization effect for solar distillation was demonstrated in terms of energy efficiency. The further investigation about evaporated water collection and purified water quality is required.

6.2 Future Work

A possible idea for future analysis was the addition of other materials to the DLS to make a triple layered structure (or TLS). Activated carbon has a lot of applications as a water cleaner and can be shown in Figure 39 and Figure 40 as an efficient cleaner for MFF wastewater. These two figures were actual tests of the material by mixing the activated carbon for 24 hours with the partially treated waste water. Distillation, however, was not explored and the idea of using that to improve the water cleaning capabilities of the DLS would be very useful research. A possible

theory is that the carbon materials used in this process may act like activated carbon to absorb contaminants but a lack of further samples of wastewater prevented clarifying this theory. Further study on this would be invaluable to understand how carbon distillation works.

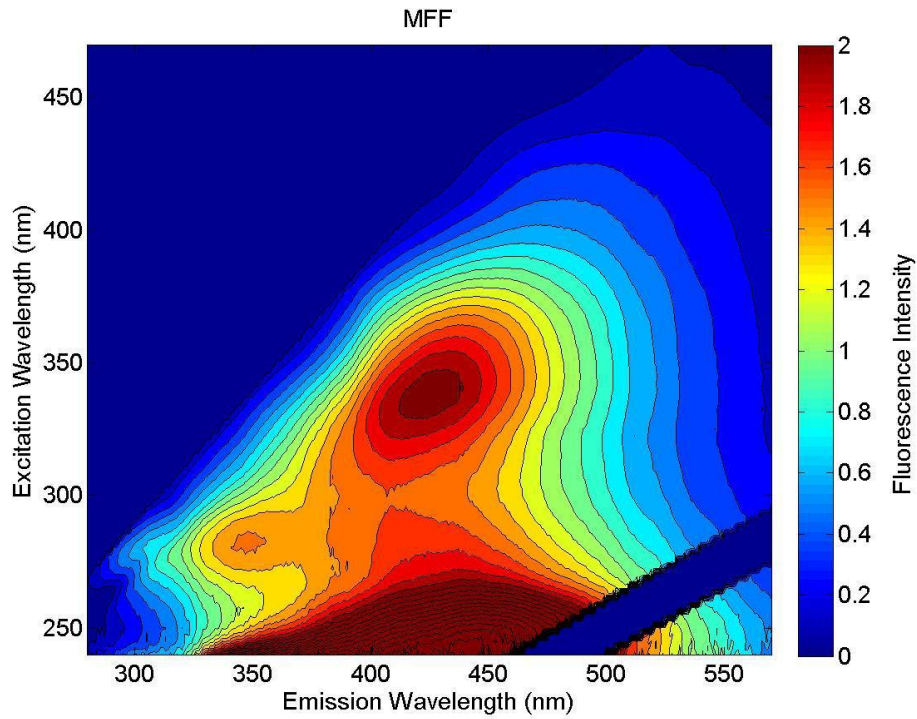


Figure 39: Initial MFF wastewater fluorescence absorbance

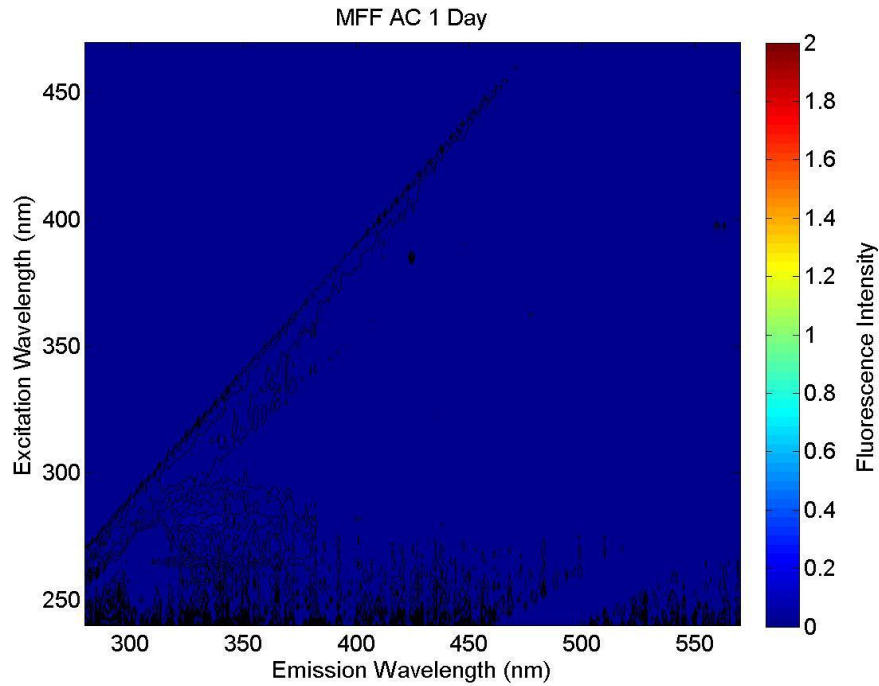


Figure 40: Final fluorescence of MFF after activated carbon exposure

Another major application is a larger scale evaporation setup. The recordings of mass change were measured in kilograms per meter squared. The idea of this measurement is to be able to multiply this value to calculate either a new mass rate or a quantity of mass obtained from a similar setup. Figure 41 shows an acrylic box that was developed for larger scale testing of water collection. If a larger area of material was used for this box, more water should be obtained either for steam generation or distillation.



Figure 41: An example of an acrylic larger scale solar distiller

Appendix

Appendix A: Material Candidates

Table 4: Various research nanomaterials candidates for solar distillation application.

Potential Nanomaterials and Properties					
Material	Thermal Conductivity (W/m*k)	Density (g/cm ³)	Hydrophilic	Solar absorption	Top or bottom layer candidate
Cobalt Oxide (CoO)	2.3-3.5	6.44	Yes	200-1,000 nm	Top
Titanium Oxide (TiO ₂)	4.8-11.8	4.05	Yes	200-700 nm	Top
Aerogel	0.017	0.003	Yes (made hydrophilic)	N/A	Bottom
Mesoporous zeolites	1	0.8-2.4	Yes	N/A	Bottom
Polyethylene	0.06	0.91-0.96	Yes (made hydrophilic)	N/A	Bottom

Appendix B: LabVIEW Block Diagrams

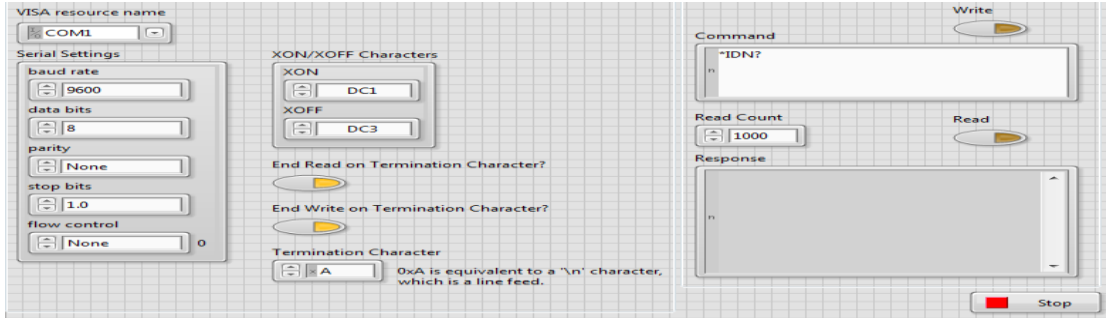


Figure 42: VI for mass change

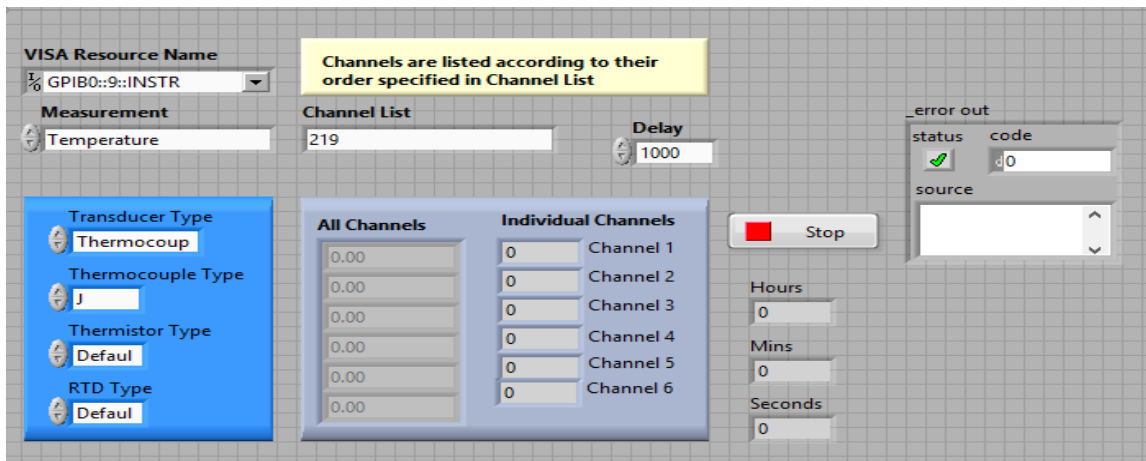


Figure 43: VI for temperature recording

Appendix C: Autodesk Inventor Drawings for Test Chamber

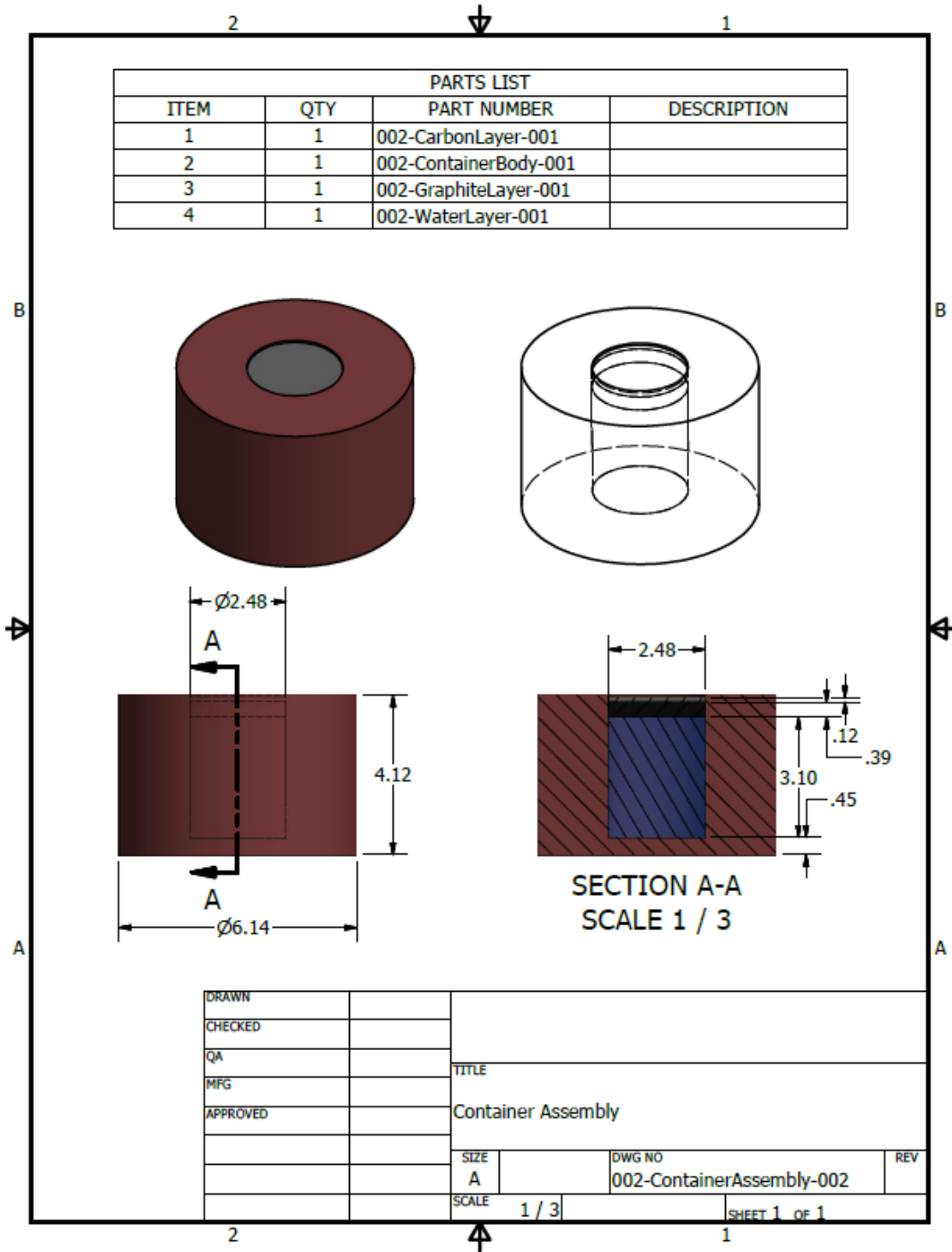


Figure 44: The test chamber model used for analysis with water and DLS

Appendix D: PLT Metal Halide Lamp Datasheet

400 Watt Probe Start Lamp **PLT-991327**
STANDARD PROBE START METAL HALIDE LIGHTING SYSTEM DATA SHEET

PRECISION
Lighting & Transformer



T15



- Dia. - 1.81" (46mm)
- MOL - 9.75" (248mm)
- LCL - 5.75" (146mm)
- Base - Mogul (E39)

MH400/T15/HOR/4K

GENERAL Characteristics

Lamp Type	Standard MH Single Ended
ANSI Code	M59/E
Bulb Shape	T15
Base Type	Mogul (E39)
Bulb Finish	Clear
Rated Life	15000 hours
Operating Position	Horizontal ± 15°

ELECTRICAL

Lamp Watts	400
Lamp Oper. Voltage (Nom.)	135

SUSTAINABILITY

Recycling Program	
-------------------	--

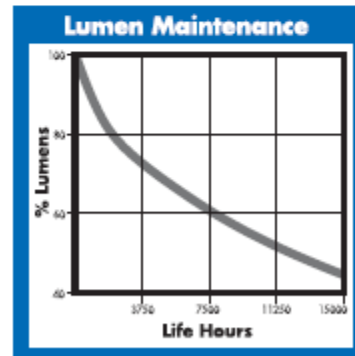
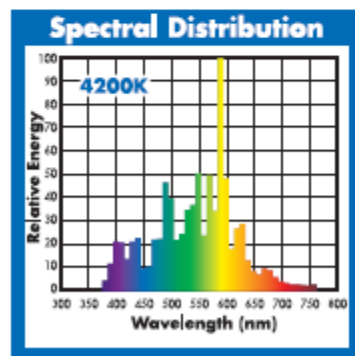
NOTES

PHOTOMETRIC

Initial Lumens	36000
Lumens Per Watt	90
Scotopic Lumens (SIP 1.7)	61200
Lamp Lumen Depreciation (LLD) .65 (65%) @ 6000 hours	
Correlated Color Temperature	4200K
Chromaticity Coordinates (CIE-x,y)	.380 .377
Color Rendering Index (CRI)	65

PHYSICAL

Bulb Diameter	1.81" (46mm)
Max. Overall Length (MOL)	9.75" (248mm)
Light Center Length (LCL)	5.75" (146mm)
Effective Arc Length	39 mm
Max. Base Temperature (°C)	210
Max. Bulb Temperature (°C)	480
Socket Pulse Rating (KV)	-
Luminaire Type	Enclosed Rated



THIS LAMP CONFORMS TO FEDERAL STANDARD 21 CFR 1040.30

Warnings: This lamp can cause skin burn and eye inflammation from shortwave ultraviolet radiation if outer envelope of the lamp is broken or punctured. Do not use where people will remain for more than a few minutes unless adequate shielding or other safety precautions are used. Lamps that will automatically extinguish when outer envelope is broken or punctured are commercially available.

Revision: 8/24/2011

Figure 45: Datasheet for metal halide lamp provided by PLT

Appendix E: Autodesk Inventor Drawings for Metal Halide Lamp Setup



Figure 46: CAD model of the metal halide (ANSI: M59) light bulb

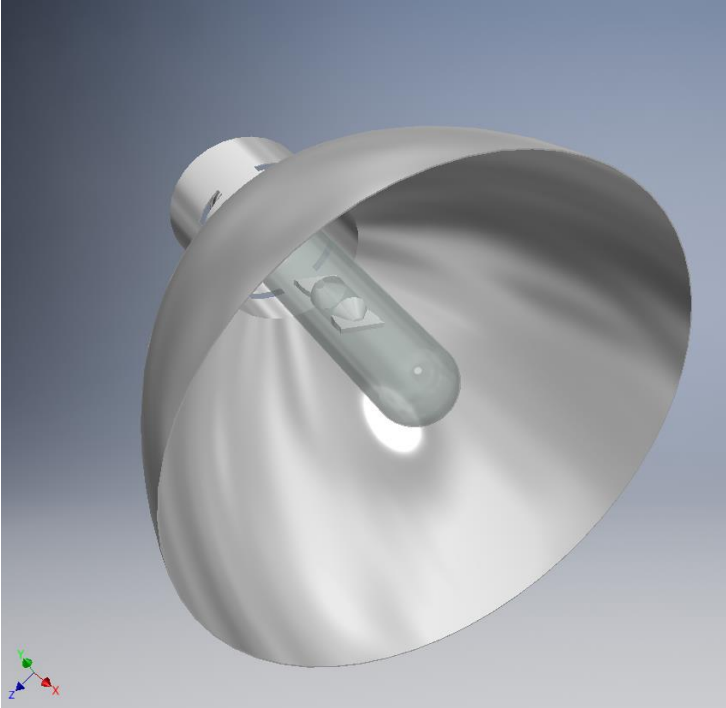


Figure 47: The reflector combined with the metal halide bulb

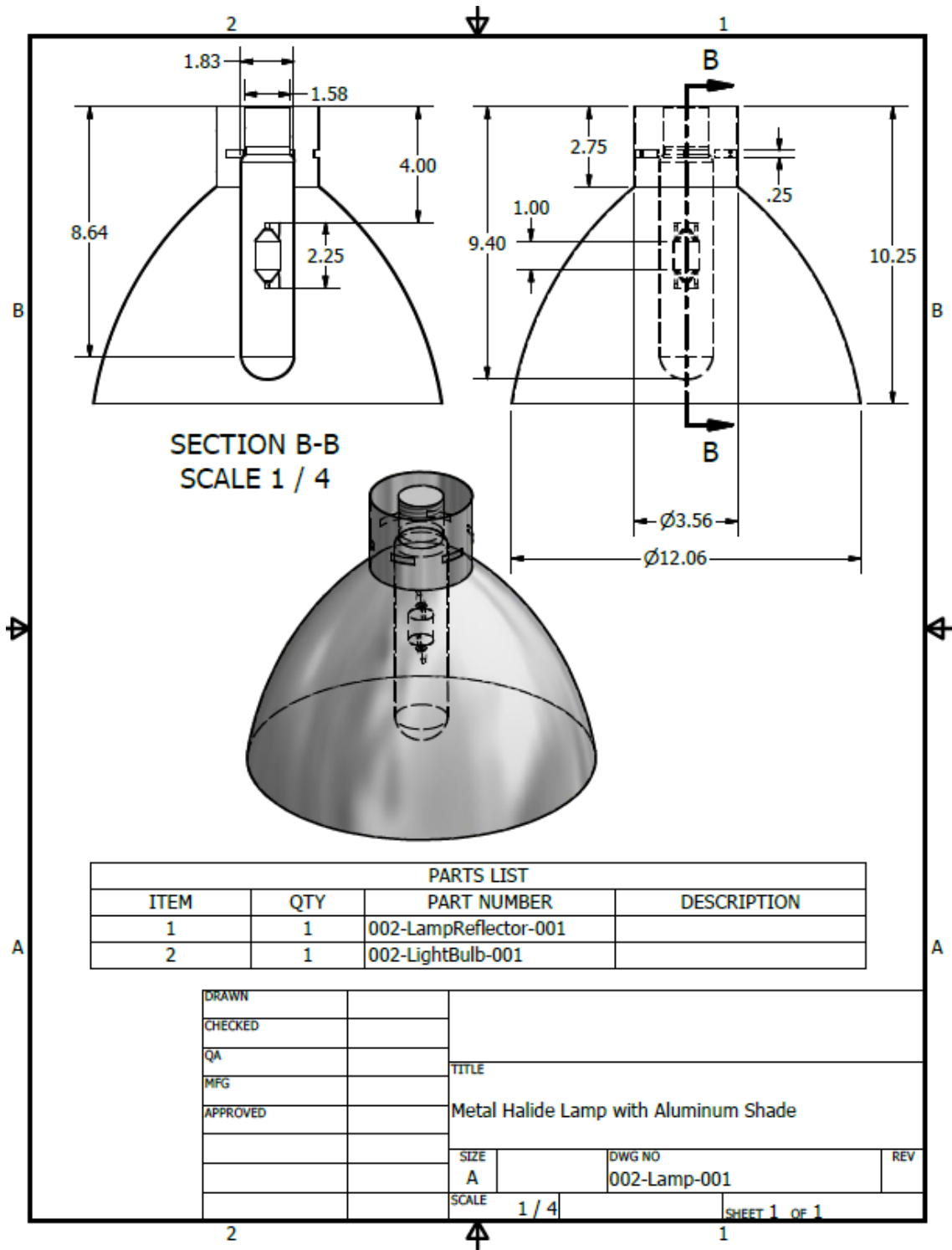


Figure 48: CAD drawings with dimensions for lamp with reflector

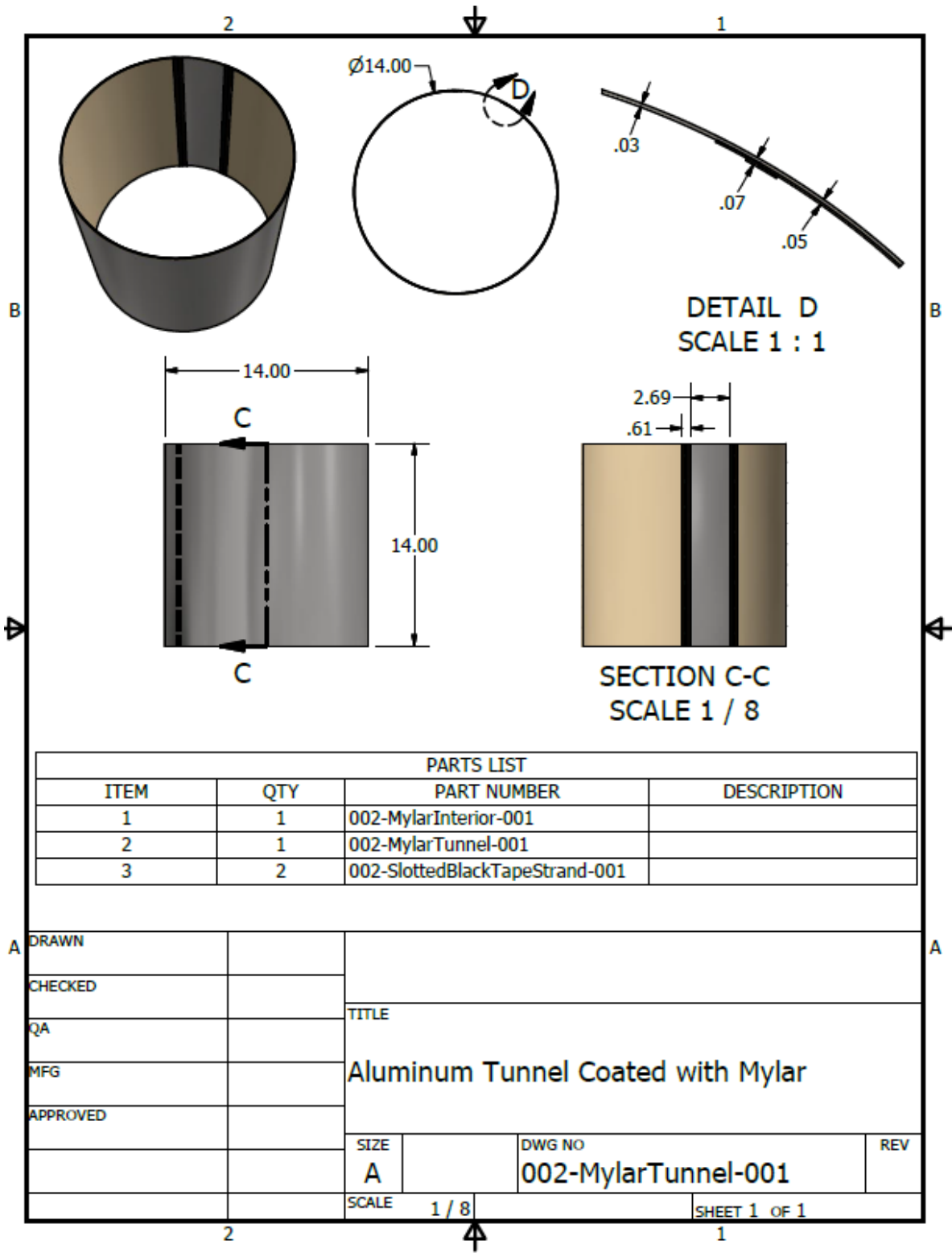


Figure 49: CAD drawing of Mylar tunnel

Appendix F: Optical Setup

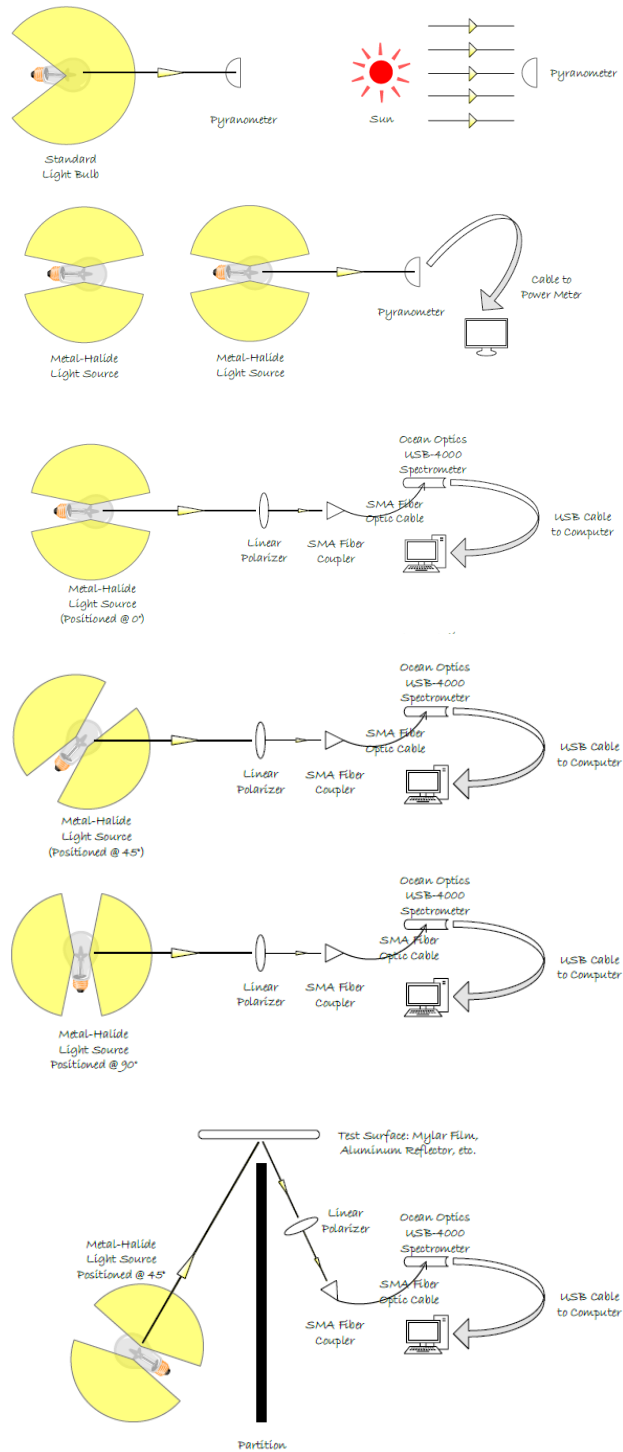


Figure 50: Optical setup for the spectrometer readings

Bibliography

- Al-Hamadani, A. A., & Shukla, S. K. (2014). Experimental Investigation and Thermodynamic Performance Analysis of a Solar Distillation System with PCM Storage: Energy and Exergy Analysis. *Distributed Generation & Alternative Energy Journal*, 29(4), 7-24. doi:10.1080/21563306.2014.11442728
- Al-Hayeka, Imad, and Omar O. Badran. "The effect of using different designs of solar stills on water distillation." *Desalination* 169.2 (2004): 121-127.
- Arunkumar, T., Jayaprakash, R., Denkenberger, D., Ahsan, A., Okundamiya, M., kumar, S., & ... Aybar, H. (2012). An experimental study on a hemispherical solar still. *Desalination*, 286342-348. doi:10.1016/j.desal.2011.11.047
- Bhardwaj, R., ten Kortenaar, M., & Mudde, R. (2015). Maximized production of water by increasing area of condensation surface for solar distillation. *Applied Energy*, 154480-490. doi:10.1016/j.apenergy.2015.05.060
- Codd, D. S., Carlson, A., Rees, J., & Slocum, A. H. (2010). A low cost high flux solar simulator. *Solar Energy*, 84(12), 2202-2212. doi:10.1016/j.solener.2010.08.007
- Cohen-Tanugi, David, and Jeffrey C. Grossman. "Water desalination across nanoporous graphene." *Nano letters* 12.7 (2012): 3602-3608.
- Elango, T., Kannan, A., & Kalidasa Murugavel, K. (2015). Performance study on single basin single slope solar still with different water nanofluids. *Desalination*, 36045-51. doi:10.1016/j.desal.2015.01.004
- Fath, Hassan ES. "Solar distillation: a promising alternative for water provision with free energy, simple technology and a clean environment." *Desalination* 116.1 (1998): 45-56.)
- FRED Optical Engineering Software version XX.XXX.X, Photon Engineering LLC, Tucson, AZ, United States.
- Ghasemi, H., Ni, G., Marconnet, A. M., Loomis, J., Yerci, S., Miljkovic, N., & Chen, G. (2014). Solar steam generation by heat localization. *Nature Communications Nat Comms*, 5. doi:10.1038/ncomms5449
- Gilmore, A. (n.d.). HORIBA - Water-Quality Measurements with the HORIBA Scientific AquaLog®. Retrieved May 18, 2016, from <http://www.spectroscopyonline.com/horiba-water-quality-measurements-horiba-scientific-aqualog>

- Hu, H., Zhao, Z., Zhou, Q., Gogotsi, Y., & Qiu, J. (2012). The role of microwave absorption on formation of graphene from graphite oxide. *Carbon*, 50(9), 3267-3273.
- Kabeel, A. E., Omara, Z. M., & Essa, F. A. (2014). Improving the performance of solar still by using nanofluids and providing vacuum. *Energy Conversion & Management*, 86268-274. doi:10.1016/j.enconman.2014.05.050
- KALITA, P., DEWAN, A., & BORAH, S. (2016). A review on recent developments in solar distillation units. *Sadhana*, 41(2), 203-223.
- Koning, J. D., & Thiesen, S. (2005). Aqua Solaris – an optimized small scale desalination system with 40 litres output per square meter based upon solar-thermal distillation. *Desalination*, 182(1-3), 503-509. doi:10.1016/j.desal.2005.03.026
- Lewis, N. S. (2007, February 09). Toward Cost-Effective Solar Energy Use. Retrieved April 19, 2016, from <http://science.sciencemag.org/content/315/5813/798.full>
- Macedonio, F., Drioli, E., Gusev, A., Bardow, A., Semiat, R., & Kurihara, M. (2012). Efficient technologies for worldwide clean water supply. *Chemical Engineering and Processing: Process Intensification*, 51, 2-17. doi:10.1016/j.cep.2011.09.011
- Morad, M., El-Maghawry, H. A., & Wasfy, K. I. (2015). Improving the double slope solar still performance by using flat-plate solar collector and cooling glass cover. *Desalination*, 3731-9. doi:10.1016/j.desal.2015.06.017
- Sampathkumar, K., et al. "Active solar distillation—a detailed review." *Renewable and Sustainable Energy Reviews* 14.6 (2010): 1503-1526.
- Sharon, H., & Reddy, K. (2015). Performance investigation and enviro-economic analysis of active vertical solar distillation units. *Energy*, 84794-807. doi:10.1016/j.energy.2015.03.045
- Stankovich, S., Dikin, D. A., Piner, R. D., Kohlhaas, K. A., Kleinhammes, A., Jia, Y., . . . Ruoff, R. S. (2007). Synthesis of graphene-based nanosheets via chemical reduction of exfoliated graphite oxide. *Carbon*, 45(7), 1558-1565. doi:10.1016/j.carbon.2007.02.034
- Taamneh, Y., & Taamneh, M. M. (2012). Performance of pyramid-shaped solar still: Experimental study. *Desalination*, 29165-68. doi:10.1016/j.desal.2012.01.026
- Tiwari, G. N., H. N. Singh, and Rajesh Tripathi. "Present status of solar distillation." *Solar energy* 75.5 (2003): 367-373.

Tsyntsarski, B., Petrova, B., Budinova, T., Petrov, N., Velasco, L. F., Parra, J. B., & Ania, C. O. (2012). Porosity development during steam activation of carbon foams from chemically modified pitch. *Microporous and Mesoporous Materials*, 154, 56-61. doi:10.1016/j.micromeso.2011.08.023

Water for Life: Making it Happen (PDF). World Health Organization and UNICEF. 2005. ISBN 92-4-156293-5.

Curriculum Vitae

Jack Cheney

6551 Annie Oakley Dr. Apt. 414

Henderson, NV 89014

702-354-6534

Cheneyj4@unlv.nevada.edu

www.linkedin.com/pub/jack-cheney/57/4b4/411/

OBJECTIVE

To pursue a Master's in Mechanical Engineering with a focus on completing a thesis regarding mechanics in materials for solar distillation.

EDUCATION

Bachelor of Science in Mechanical Engineering

University of Nevada, Las Vegas (UNLV) (May 2014)

Minor in Solar and Renewable Energy

EMPLOYMENT

Graduate Assistantship at UNLV (August 2014 to present)

- Graded homework in an orderly and timely fashion and provided help to students when requested
- Taught a lab class every two weeks and provided further help beyond the class in writing lab reports
- Tutored students within engineering disciplines on a scheduled basis
- Provided a review session for a class on Fridays that was completely customized for students to help understand the material
- Conducted experimental work for solar water distillation attended weekly meetings while continuing studies within Master's degree

Solar System Design Engineer at Bombard Renewable Energy (July 2013-August 2014)

- Developed strong understanding of PVSyst software
- Extensive experience with developing Excel template for predicting solar output and cost
- Performed various other duties such as AutoCAD roof design and database analysis of solar data on DECK website
- Promoted integration of solar systems through social media and community outreach events

RESEARCH EXPERIENCE

Graduate Assistant

Thesis research funded by Dr. Jaeyun Moon for NEXUS Solar Distillation Project (August 2014-Present)

- Substantial research on nanomaterials for use as heat transfer facilitator
- Design criteria for water distillation using solar power
- Construction of water collector box and LabVIEW programming

- Weekly updates of research, monthly reports, and periodic literature reviews
- Work with other colleagues as a collaborative team with task distribution

Volunteer

Engineer and construction participate in building UNLV's DesertSol for Solar Decathlon 2013 (2nd overall, 1st nationally) (2012-2013)

- Researched on solar thermal water heater time requirements for evacuated tubes to heat to 120 degrees Fahrenheit
- Provided "green tips" and other blog entries that incorporate sustainable living on the website
- Studied solar evacuated tubes using Datalogger Software and analyzed efficiency of DesertSol solar thermal system for solar water heater and completed analysis of heat output through Excel programming
- Contributed 100+ hours towards construction and promotion of the home

AWARDS

- Summer Research Assistantship (June 2015-August 2015)
- Graduate Assistantship (August 2014-Present)
- O'Rourke Plumbing Scholarship (2013, 2014)
- Provost Scholarship (2009-2013)
- Millennium Scholarship (2009-2014)
- Dean's List of College of Engineering (2009)

PROFESSIONAL AFFILIATIONS

- Society of Asian Scientist and Engineers (SASE), Member
- American Society of Mechanical Engineers (ASME), Member
- National Society of Professional Engineer (NSPE), Member

References available upon request